Coordinated Beamforming for Millimeter-wave Terrestrial Peer-to-Peer Communication Networks

Aaron J. Marinkovich

Thesis submitted to the faculty of the Virginia Polytechnic Institute and State University in partial fulfillment of the requirements for the degree of

Master of Science
In
Electrical Engineering

Steven W. Ellingson, Chair
Richard M. Buehrer
Harpreet S. Dhillon

September 11, 2020
Blacksburg, Virginia

Keywords: Coordinated Beamforming, Beamforming, Millimeter-wave Communication, Peer-to-Peer Communication, Terrestrial Communication Network

Coordinated Beamforming for Millimeter-wave Terrestrial Peer-to-Peer Communication Networks

Aaron J. Marinkovich

ABSTRACT

Terrestrial mobile peer-to-peer millimeter wave networks will likely use beamforming arrays with narrow beams. Aligning narrow beams is difficult. One consideration for aligning narrow beams is co-channel interference. Beams can be aligned either on a per-link basis where co-channel interference is ignored, or on a global basis where co-channel interference is considered. One way to align beams on a global basis is coordinated beamforming. Coordinated beamforming can be defined as alignment of beams on a global basis, so as to jointly optimize the signal-to-interference-plus-noise ratio (SINR) of all links operating in a network. In this work, we explore coordinated beamforming in peer-to-peer networks and demonstrate its efficacy. Networks with varying numbers of links are simulated in scenarios with and without obstructions. The coordinated beamforming schemes presented in this work significantly improve link SINR statistics in these scenarios. Greater improvement was found in networks with higher numbers of links and in networks in terrain with obstructions.

Coordinated Beamforming for Millimeter-wave Terrestrial Peer-to-Peer Communication Networks

Aaron J. Marinkovich

GENERAL AUDIENCE ABSTRACT

Wireless communication links can interfere with each other. Interference can be mitigated by adjusting the antennas with which the links are formed. One method of mitigating interference is coordinated beamforming. Coordinated beamforming can be defined as a method of adjusting antennas to jointly optimize the strength of the links operating in a network. In this work, we explore coordinated beamforming in terrestrial mobile peer-to-peer communication networks and demonstrate its efficacy. Networks with varying numbers of links are simulated in scenarios with and without obstructions. The coordinated beamforming schemes presented in this work significantly improve link strength statistics in these scenarios. Greater improvement was found in networks with higher numbers of links and in networks in terrain with obstructions.

Contents

List of Tables

List of Figures

Chapter 1

Introduction

Future terrestrial mobile wireless communication networks will likely operate in the millimeter wave band (30 GHz-300 GHz), see e.g. [1]. Millimeter waves experience at least 20 dB more free-space path loss than UHF waves. Mobile millimeter wave networks will use beamforming arrays to compensate for this additional loss.

These beamforming arrays will have narrow beams, which are difficult to align. Another consideration when aligning beams is co-channel interference. Beams can be aligned on a per-link basis where co-channel interference is ignored. We refer to beam alignment schemes that form links without regard for the co-channel interference between links as "pairwise schemes." Alternatively, beams can be aligned to account for co-channel interference to and from nearby links. We refer to beam alignment schemes that account for co-channel interference as "global schemes." Global schemes can be viewed as coordinated beamforming schemes. We define coordinated beamforming as the selection of beam pointings and transmitter powers to globally optimize the signal-to-interference-plus-noise ratios (SINR) of links. In this thesis, we explore coordinated beamforming in peer-to-peer networks and analyze its efficacy.

This chapter is organized as follows. A common beam alignment method, beam scanning, is presented in Section 1.1. An overview of this thesis is presented in Section 1.2. Contributions are presented in Section 1.3. The organization of the remainder of this thesis is

presented in Section 1.4.

1.1 Beam Scanning

The principal difficulty posed by narrow beams is beam alignment. Generally insufficient knowledge of mutual positions and terrain is available for deterministic beam alignment. Instead, "beam scanning" is typically proposed, see e.g. [2]. Beam scanning is beam alignment by testing many pointings over a broad angular range. The principal drawbacks of beam scanning are (1) latency and (2) co-channel interference. Concerning latency, several pointings might be tested before a pointing that yields a viable link is found. Concerning co-channel interference, stations create co-channel interference as they test their pointings. Coordinated beamforming potentially avoids both problems, although MS positions and terrain knowledge are required. In this work, we consider the efficacy of coordinated beamforming with and without knowledge of terrain.

1.2 Overview of Thesis

An illustration of the scenario addressed in this thesis is shown in Figure 1.1. Networks consist of multiple, independent links between mobile stations (MS). An illustration of a MS in this study is shown in Figure 1.2. MSs are ground vehicles equipped with beamforming arrays. These beamforming arrays have fixed antenna patterns that can be steered, i.e., beam shaping is not considered in this study. We assume that perfect knowledge of MS location and antenna orientation is available. Each MS is associated with only one link. Unintended transmission between links is co-channel interference. For the purposes of this study, each MS is designated either a transmitter MS or a receiver MS.

Terrestrial networks will likely be in environments with obstructions that block line-of-sight (LOS) paths, see e.g. [1]. These obstructions could also potentially be used to form links along non-line-of-sight (NLOS) paths via reflection. We define the set of obstructions,

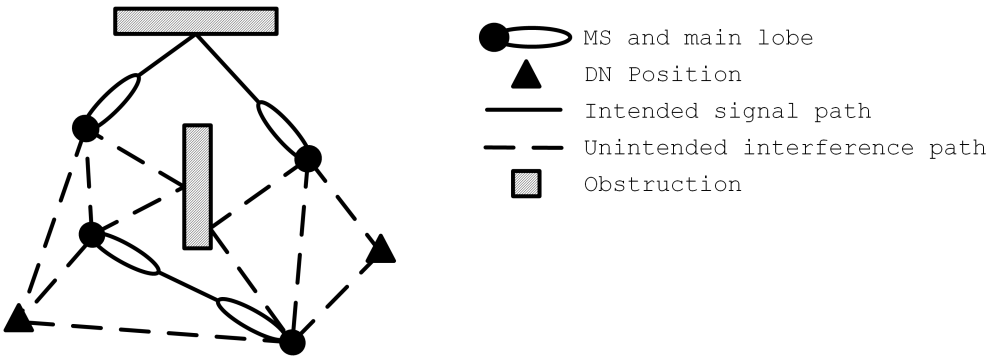

Figure 1.1: Illustration of scenario addressed in this thesis.

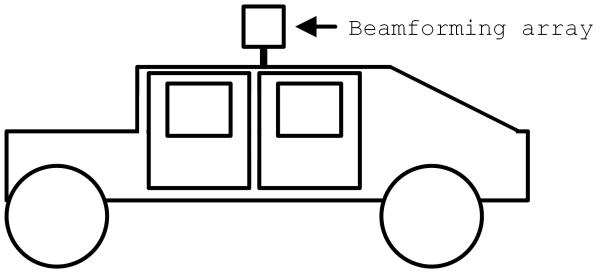

Figure 1.2: Illustration of a MS in this study.

including buildings, vehicles, and hills as "terrain." The efficacy of coordinated beamforming in a variety of terrain is considered in this thesis.

Desired null (DN) positions are defined as positions where received power is ideally zero. DN positions may represent eavesdroppers within a network. Coordinated beamforming methods may reduce the potential for eavesdroppers to detect and intercept communication between MSs. This could be accomplished by minimizing the power incident at DN positions. The efficacy of coordinated beamforming to minimize power incident at DN positions is considered in this thesis. However, the coordinated beamforming methods presented in this thesis prioritize globally optimizing link SINRs in the network over minimizing power incident at DN positions, as explained in Sections 3.2.

An illustration of the problem statement of this thesis is shown in Figure 1.3. Coordi-

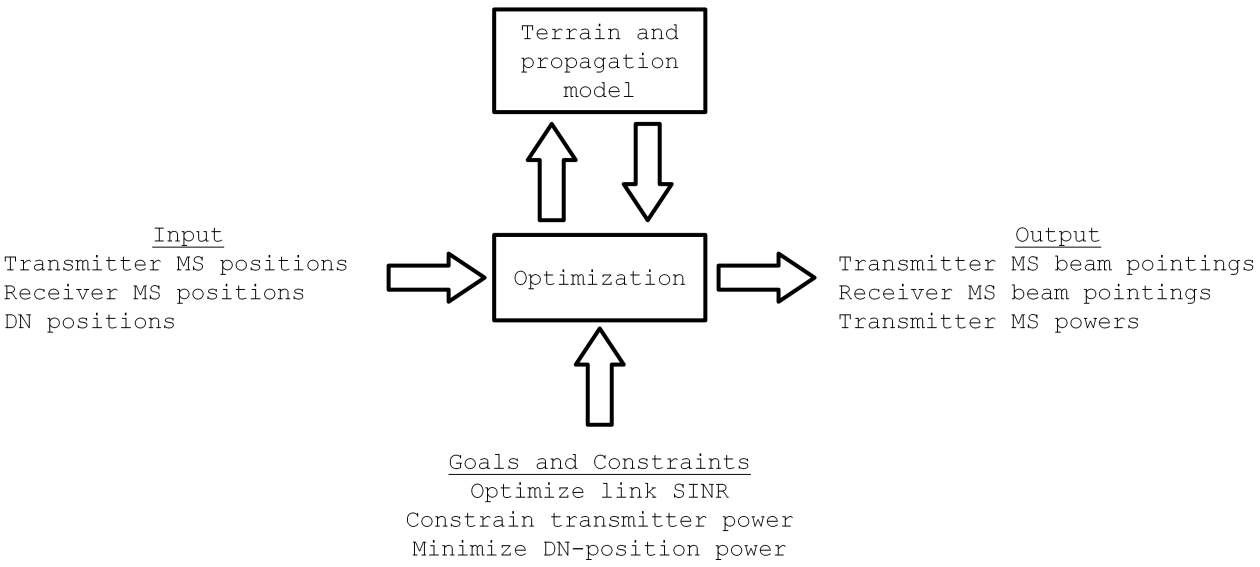

Figure 1.3: Illustration of problem statement of this thesis.

nated beamforming methods select beam pointings and transmitter powers given MS positions, DN positions, and terrain information. The criteria for selecting beam pointings and transmitter powers are based on link SINR, transmitter power levels, and powers incident at DN positions. These criteria are used to define a constrained optimization problem, which is presented in Section 3.2.

A closed form solution to the constrained optimization problem is not available, so a search is required. The global schemes presented in this thesis use a brute-force search, which is defined as a search that evaluates every solution within a (possibly limited) search space of solutions. Even when the solution space is limited, performing an exhaustive search that guarantees the optimum solution is found is intractable, as explained in Section 3.3. Consequently, techniques to discretize the solution space are considered, as explained in Section 3.4.

The family of schemes presented in this thesis is presented in Table 1.1. A variety of pairwise and global schemes with different assumptions concerning terrain knowledge are analyzed. Pairwise schemes are used to establish a baseline of performance to compare with the performance of global schemes. Null terrain is defined as flat terrain without obstructions. Schemes that assume null terrain are the "Pairwise Assuming Null terrain" (PAN) scheme and "Global Assuming Null terrain" (GAN) scheme. Schemes that assume perfect knowledge of the

Class of scheme	**Assuming null terrain:**	**Assuming perfect knowledge of terrain is available:**
Pairwise	Pairwise Assuming Null terrain (PAN) (Section 2.2)	Pairwise assuming Perfect Knowledge of terrain (PPK) (Section 5.2)
Global	Global Assuming Null terrain(GAN) (Sections 3.2-3.5)	Global assuming Perfect Knowledge of terrain (GPK) (Section 5.3)

Table 1.1: Family of schemes presented in this thesis and their associated assumptions concerning terrain.

terrain is available are the "Pairwise assuming Perfect Knowledge of terrain" (PPK) scheme and "Global assuming Perfect Knowledge of terrain" (GPK) scheme. Each of these schemes is addressed in the sections indicated in Table 1.1.

A Monte Carlo simulation process, described in Section 2.1, was developed to evaluate these schemes. Networks with varying number of links and in different terrains are analyzed. In particular, PAN, PPK, and GPK are analyzed in realistic terrain, shown in Figure 1.4. This terrain is referred to as "residential terrain" and is described in Section 5.1.

1.3 Contributions

The contributions of this thesis are as follows.

- Developed set of computationally tractable schemes for coordinated beamforming in terrestrial mobile peer-to-peer millimeter networks, specifically GAN (Sections 3.2-3.5) and GPK (Section 5.3).
- Demonstrated efficacy and limitations of coordinated beamforming in null terrain (Figures 3.9 and 3.10, Table 3.5) and residential terrain (Figures 5.6 and 5.7, Table 5.5).
- Developed simulation framework to generate results presented in this thesis. The simulation process is described in Section 2.1. The terrain and propagation models are presented in Sections 2.1 and 4.1.

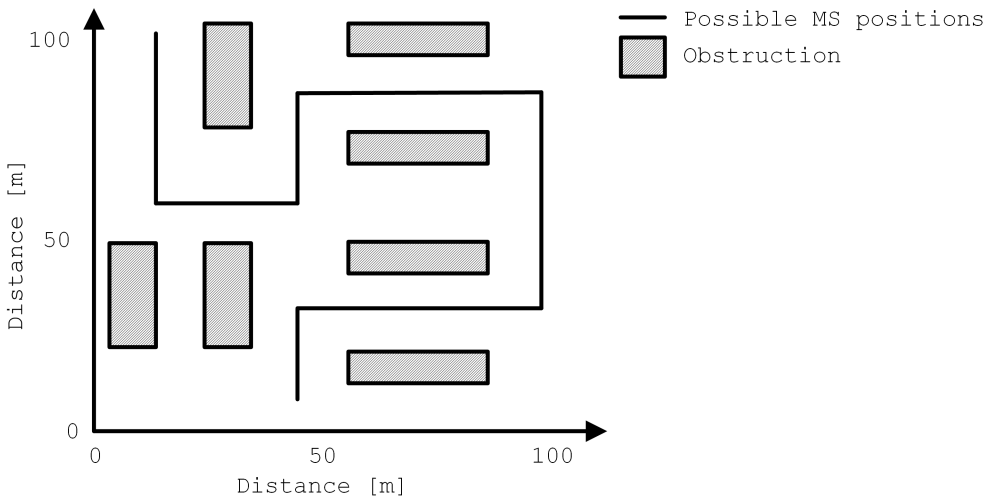

Figure 1.4: Residential terrain. As explained in Section 5.1, MSs are constrained to positions along the track as shown.

1.4 Organization of Thesis

The organization of the remainder of this thesis is as follows.

- In Chapter 2 ("Pairwise Scheme in Null Terrain"), the simulation process, propagation model, and PAN are described. Results for PAN in null terrain are presented.
- In Chapter 3 ("Global Scheme in Null Terrain"), GAN is described and results of GAN in null terrain are presented. Additionally, the computational burden of an exhaustive search is analyzed.
- In Chapter 4 ("Millimeter Wave Propagation in Presence of Obstructions"), the propagation model for millimeter waves in the presence of obstructions is presented.
- In Chapter 5 ("Pairwise and Global Schemes in Residential Terrain"), PPK and GPK are described. Results of PAN, PPK, and GPK in residential terrain are presented.
- In Chapter 6 ("Conclusions"), additional considerations are explored and future work is suggested.

Chapter 2

Pairwise Scheme in Null Terrain

A simulation of the scenario described in Section 1.2 is presented in this chapter. Communication networks comprised of mobile stations (MS) are simulated in a null terrain environment. From Section 1.2, null terrain is flat terrain and without obstructions. The pairwise scheme PAN that assumes the network is in null terrain and ignores co-channel interference is presented in this chapter.

This chapter is organized as follows. Simulation mechanics, including the antenna and propagation model, are presented in Section 2.1. PAN is formally defined in Section 2.2. The simulation scenario used to demonstrate the scheme is described in Section 2.3. Results are presented in Section 2.4.

2.1 Simulation Mechanics; Antenna and Propagation Model

The Monte Carlo simulation process is shown in Figure 2.1. The initial step is the random generation of MS and desired null (DN) positions. Then MS pointings and transmitter MS powers are selected using whichever scheme is being evaluated. Lastly, link SINR and the sum power incident at DN positions are calculated.

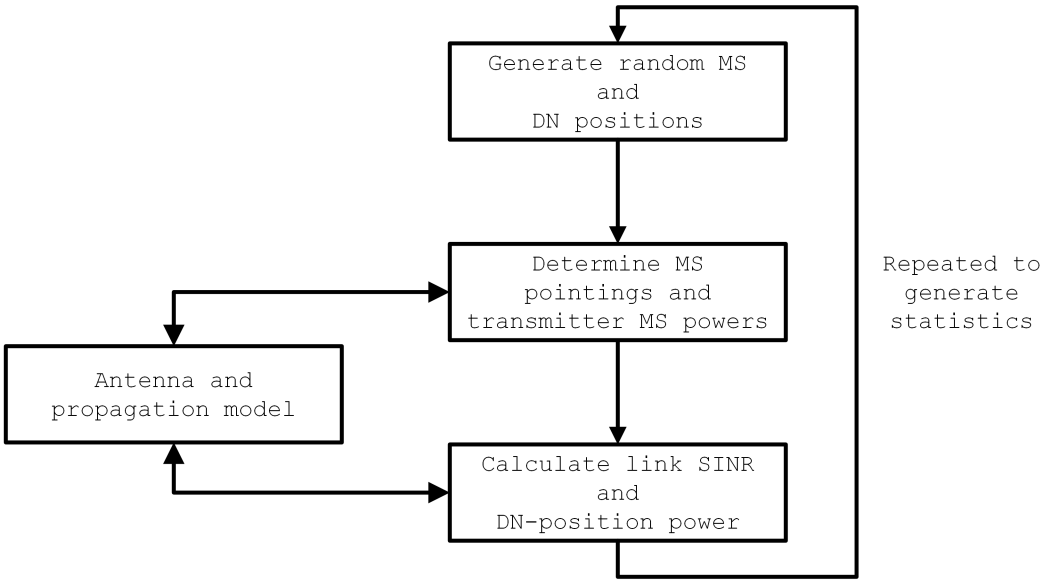

Figure 2.1: Illustration of simulation process.

The simulation process is repeated to generate statistics. The SINR and DN-position powers are complied into separate cumulative distribution functions (CDF) that are used to evaluate the performance each scheme. Expressions for these CDFs could be obtained using stochastic theory, see e.g. [3]. These closed form expressions would provide an independent check of our simulation results. However, such expressions are not available for the optimization problems considered in this thesis.

MSs are assumed to be equipped with beamforming arrays. The beamforming arrays are modeled as generic aperture antennas, see e.g. [4, Section 9.1]. One consideration for selecting an antenna model is whether the beamforming array better resembles an aperture in a perfectly-conducting ground screen or a distribution of current in free space. The models for these two types of aperture antennas exhibit a similar main lobe, but exhibit significantly different sidelobes for directions far from broadside. We choose to model the beamforming arrays as a distribution of current in free space. We further assume a uniformly-weighted vertically-polarized square-aperture antenna. The antenna geometry is shown in Figure 2.2. Thus, antenna gain G in the $x-z$ and $y-z$ planes is

$$G(\theta) = G_0 \left(\frac{\sin\left(\frac{\pi l}{\lambda}\sin\theta\right)}{\frac{\pi l}{\lambda}\sin\theta} \right)^2 \tag{2.1}$$

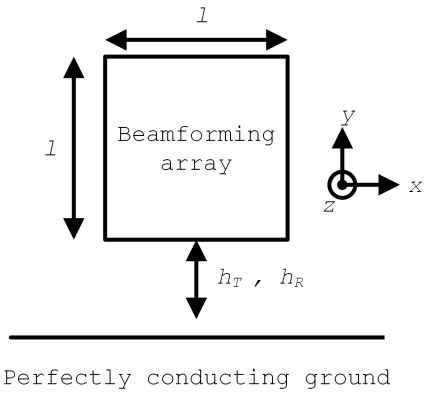

Figure 2.2: MS antenna geometry.

for $|\theta| \leq 90°$, where l denotes the antenna's side-length, λ denotes wavelength at the operating frequency, and G_0 denotes broadside antenna gain

$$G_0 \approx \frac{4\pi l^2}{\lambda^2} \tag{2.2}$$

when aperture efficiency is 100% and $l \gg \lambda$, see e.g. [4, Section 9.2.1]. Antenna gain G is assumed to be 0 for $|\theta| > 90°$.

The MS antenna patterns in the $x - z$ and $y - z$ planes for $l = 5\lambda$ are shown in Figure 2.3. This antenna creates a "sinc" antenna pattern with a first-sidelobe level (FSL) of about 13 dB. Half-power beamwidth (HPBW) for broadside pointing is

$$\text{HPBW} \approx (50.8°)\frac{\lambda}{l}. \tag{2.3}$$

In this case, HPBW $\sim 10°$, as shown in Figure 2.3.

Antennas can be steered mechanically or electrically. Antenna pattern varies with pointing when the antenna is electrically steered, see e.g. [4, Section 8.9.1]. The main lobe does not vary significantly when steered near broadside. We assume antenna pattern does not vary at all with pointing, which is accurate for mechanical steering and is a simplification for electrical steering.

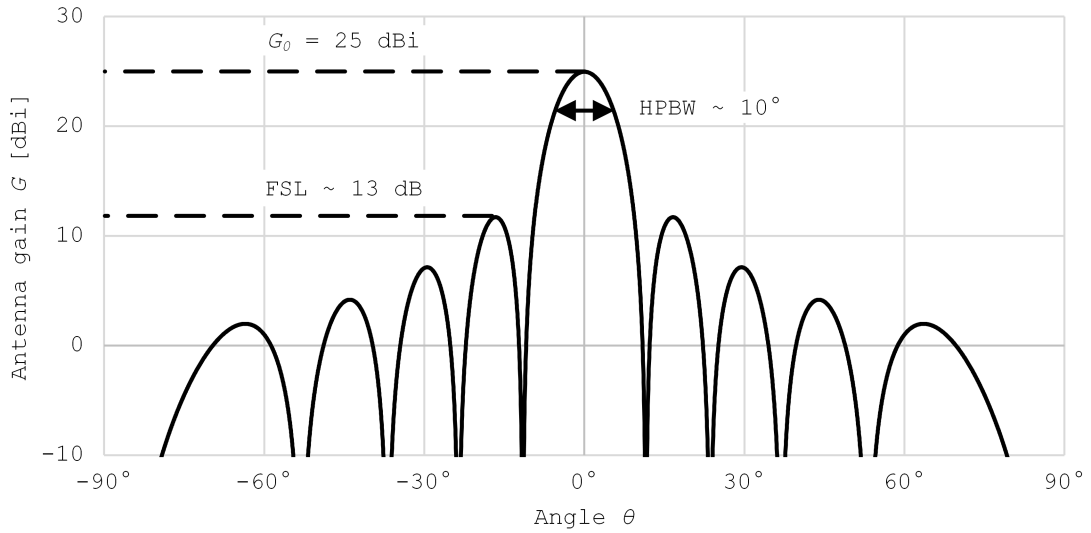

Figure 2.3: MS antenna pattern in x–z plane for broadside pointing for $l = 5\lambda$. (Pattern in y–z plane is the same.)

Received power P_R is determined by the Friis equation

$$P_R = AG_TG_RL^{-1} \tag{2.4}$$

where A denotes transmitter MS power; G_T and G_R denote transmitter and receiver antenna gain, respectively; and L denotes path loss

$$L = \left(\frac{4\pi d}{\lambda}\right)^n \tag{2.5}$$

where d denotes distance between the transmitter MS and receiver positions, and n is a scalar that varies with propagation model, see e.g. [5, Section 4.3.9]. For free space, $n = 2$. In this study, we are considering propagation over ground. The difference between propagation over ground and propagation in free space is the occurrence of "ground bounce," which is when a transmitted wave reflects from the ground before reaching the receiver. The path loss for propagation over ground (i.e., accounting for ground bounce) is nearly the same as the path loss for free space when d is much less than the "breakpoint" distance d_b

$$d_b \approx \frac{4\pi h_T h_R}{\lambda} \tag{2.6}$$

where h_T and h_R denote transmitter and receiver antenna heights above ground, respectively, see e.g. [5, Section 12.4.1]. A typical value is $\sim$ 5 km for $h_T = h_R = 2$ m and $f = c/\lambda = 30$ GHz. In this study, we restrict the $d \ll d_b$, and subsequently assume that propagation over ground exhibits $n = 2$.

2.2 PAN

The "Pairwise Assuming Null terrain" (PAN) scheme sets MS pointings and A as follows. MS antennas are pointed along line-of-sight (LOS) toward their associated MS. Transmitter power A is set to make the receiver MS's signal-to-noise ratio (SNR) equal to a specified threshold SNR.

Simulations will become burdensome, so to manage this we use a specified SNR to set A. Lower SNR is of greater interest than higher SNR given that higher SNR for one link will translate into more interference for others. With this in mind, the SNR threshold of 6 dB is chosen. This SNR corresponds to an energy-per-bit-to-noise-power-spectral-density ratio E_b/N_0 of 6 dB for a spectral efficiency of 1 bps/Hz, see e.g. [6, Section 11.2.2]. This E_b/N_0 is both relatively low for mobile radio applications yet generally high enough to support reliable communication in terrestrial fading environments using phase amplitude modulations with interleaving and forward error correction.

The SNR at a receiver is

$$\text{SNR} = \frac{AG_TG_RL^{-1}}{N} \tag{2.7}$$

where N denotes noise

$$N = kT_{sys}B \tag{2.8}$$

where k is Boltzmann's constant ($\cong 1.38 \times 10^{-23}$ J K^{-1}), T_{sys} is (receiver) system noise temperature, and B is detection bandwidth. One might choose to set A as follows:

$$A = \frac{\rho NL}{G_TG_R} \tag{2.9}$$

where ρ denotes the specified threshold SNR. However, the preceding analysis ignores interference. When A is set to make SNR equal to ρ, any amount of interference at the receiver MS will reduce the signal-to-interference-plus-noise ratio (SINR) below ρ. Interference is likely when more than one link is operating, so headroom α is included in Equation 2.9. Therefore PAN sets A as follows:

$$A \leftarrow \frac{\rho N \alpha L}{G_T G_R}. \tag{2.10}$$

2.3 Simulation Scenario

One realization of the simulation used to evaluate PAN is shown in Figure 2.4. Simulation parameters that apply to all simulations presented in this thesis are listed in Table 2.1. For these parameters, $d_b \sim 5$ km, so we restrict d to be much less than 5 km. To do so, we restrict MS positions to a circular track with a radius of 500 m. To demonstrate the simulation methodology and establish a baseline of performance for later chapters, we consider the scenarios specified in Table 2.2. Networks with three, five, and seven MS pairs are simulated. For convenience, the number of MS pairs in a network is denoted M. Every realization considered includes three randomly-determined DN positions. As stated in Section 1.2, DN positions may represent eavesdroppers in a network. Eavesdroppers could be equipped with directive antennas. However, to simplify our calculations, $G_R = 0$ dBi for computing power incident at DN positions. For all antennas $h_T = h_R$ and all antennas are pointed parallel to the ground. Link SINR and DN-position power are compiled into separate CDFs. The CDFs seemed to converge within 10,000 realizations, so we use 10,000 realizations.

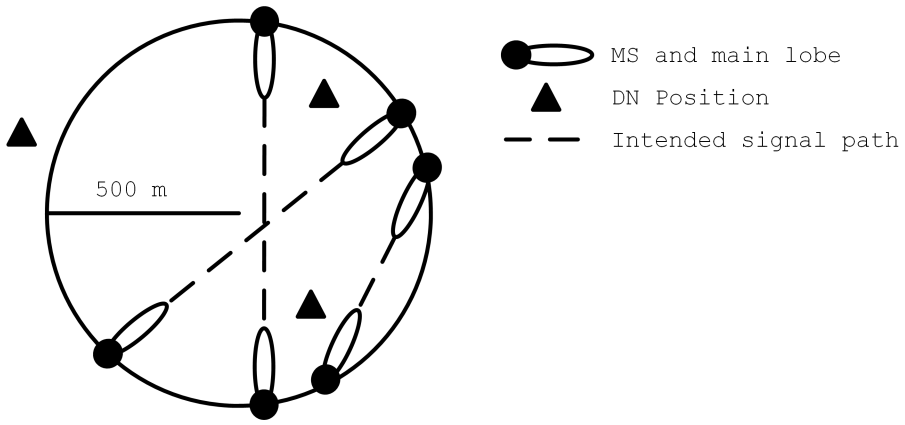

Figure 2.4: One realization of the Monte Carlo simulation.

Frequency	30 GHz
Detection Bandwidth B	1 MHz
System Noise Temperature T_{sys}	1000 K ($\sim$ 7 dB noise figure)
SNR Threshold ρ	6 dB
Headroom α	1 dB
MS Antenna	
Model	Square aperture, side-length $l = 5\lambda = 5$ cm
Broadside Gain G_0	25.0 dBi
Pattern	Sinc pattern, FSL $\sim$ 13 dB, HPBW $\sim 10^\circ$
Antenna Height Above Ground $h_T = h_R$	2 m

Table 2.1: Simulation parameters for all simulations presented in this thesis.

Terrain	Null Terrain
MS positions	Restricted to circular track, radius = 500 m
# of MS pairs M	3, 5, 7
# of DN positions	3 randomly placed
# of realizations	10,000

Table 2.2: Simulation parameters for networks in null terrain.

2.4 Results

CDFs of link SINR are presented in Figure 2.5. Note PAN constrains SINR to be less than $\rho\alpha = 7$ dB. The fractions of links that exhibit SINR < 6 dB are presented in Table 2.3. As anticipated, SINR generally decreases as M increases. This is due to the higher amounts of interference associated with higher M.

As will be explained in Chapter 3, our global schemes are designed to lower the fractions of links that exhibit SINR < 6 dB. From Table 2.3, the fractions of links that exhibit SINR < 6 dB for PAN in null terrain are between 2% and 9%. Subsequently, the potential for improvement in this respect is limited to a few percent. Changes in plots of a few percent are easier to read on a logarithmic scale. So the CDFs of link SINR plotted on a logarithmic scale are presented in Figure 2.6.

CDFs of DN-position power are presented in Figure 2.7. As anticipated, DN-position power increases as with M. Again, this is due to higher amounts of interference associated with higher M. For simplicity, we chose an arbitrary threshold equal to $N \sim -108$ dBm (Equation 2.8) to distinguish possibly-useable links from probably-unusable links. The fractions of DN-position power < -108 dBm are listed in Table 2.4. These fractions are less than 1%, regardless of M. Thus there is not much room for improvement in this aspect.

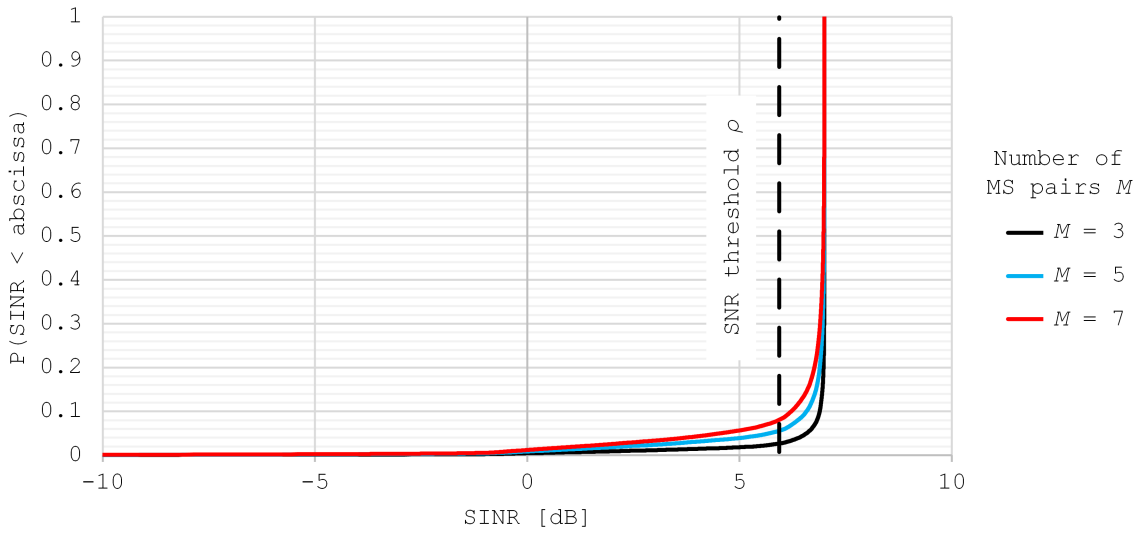

Figure 2.5: CDFs of link SINR for PAN in null terrain.

Number of MS Pairs M	**Links that exhibit SINR $<$ 6 dB**
3	2.8%
5	5.8%
7	8.4%

Table 2.3: Fractions of links that exhibit SINR $<$ 6 dB for PAN in null terrain.

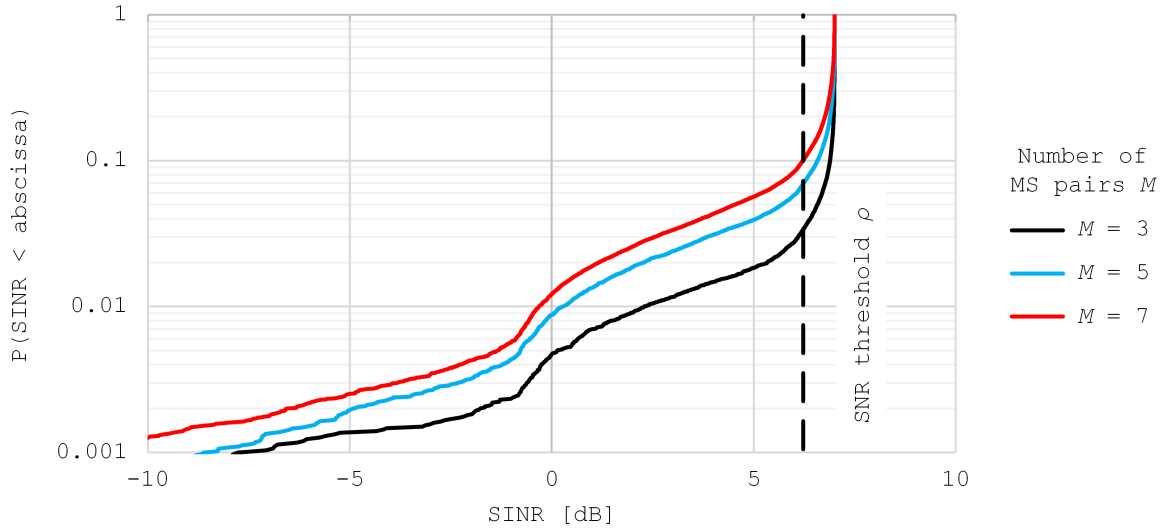

Figure 2.6: Repeating CDFs of link SINR for PAN in null terrain on a logarithmic scale.

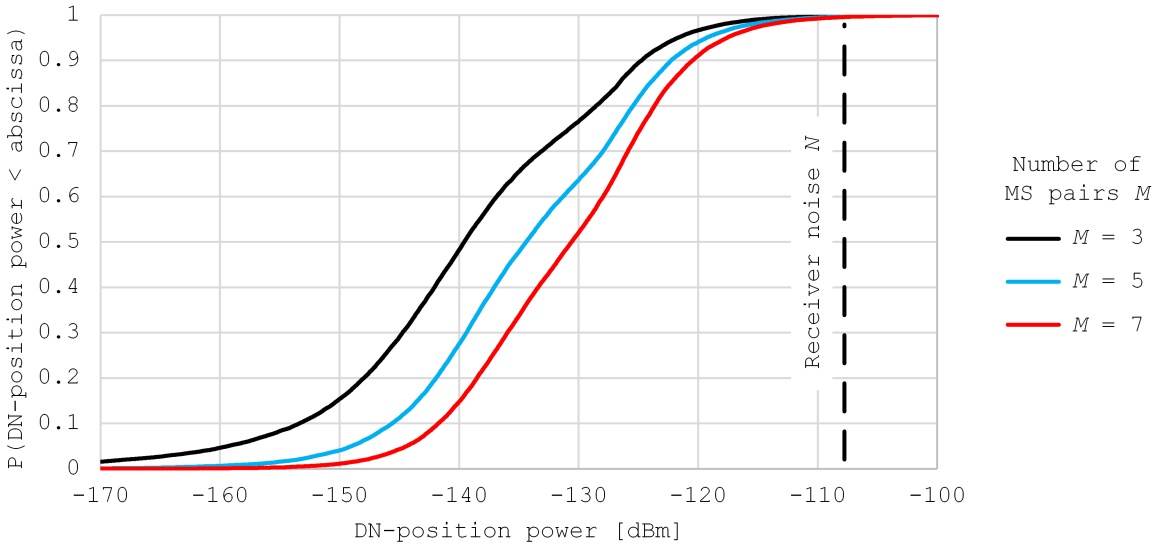

Figure 2.7: CDFs of DN-position power for PAN in null terrain.

Number of MS Pairs M	**DN-position power < -108 dBm**
3	99.8%
5	99.7%
7	99.5%

Table 2.4: Fractions of DN-position power < -108 dBm for PAN in null terrain.

Chapter 3

Global Scheme in Null Terrain

A simulation of a wireless communication network was presented in Chapter 2. Also presented in Chapter 2 was a pairwise scheme that selects mobile station (MS) pointings and transmitter MS powers without considering interference from non-associated transmitter MSs. In this chapter, we consider a global scheme, referred to as the Global Assuming Null terrain (GAN) scheme, which (repeating from Section 1.2):

- Provides sufficient signal power at associated receiver MSs to meet a specified threshold signal-to-interference-plus-noise ratio (SINR), i.e., interference from non-associated transmitter MSs is explicitly considered.
- Attempts to minimize interference at non-associated receiver MSs and desired null (DN) positions.

Simulations analogous to those presented in Chapter 2 are performed using GAN. Once again, simulated networks are in a "null terrain" environment.

This chapter is organized as follows. The global scheme presented in this chapter is defined in terms of a constrained optimization problem. Approaches to constructing a constrained optimization problem for a coordinated beamforming scheme are presented in Section 3.1. The constrained optimization problem is presented in Section 3.2. A closed form

solution is not available, so we consider a brute-force search method that evaluates every possible solution. This turns out to be intractable, so we determine the smaller number of candidate solutions that the scheme can evaluate within a reasonable amount of time, which is presented in Sections 3.3-3.5. Simulation results are presented in Section 3.6. Conclusions are presented in Section 3.7.

3.1 Constructing a Constrained Optimization Problem

There are multiple approaches to constructing a constrained optimization problem for a coordinated beamforming scheme. One approach is to maximize sum capacity while constraining the sum of transmitted powers in a network; for an example, see e.g. [7]. Another approach is to minimize the sum of transmitted powers in a network while constraining the solution space to only include solutions with links that exhibit SINR above a specified threshold; for an example; see e.g. [8], where it is shown that this approach leads to a relatively low complexity method of solution. In the present work, we aim to minimize the highest individual transmitter power level while constraining SINR to be above a specified threshold.

3.2 GAN

GAN is defined in terms of the following constrained optimization problem:

$$\min(\max(\mathbf{A})) \quad \text{such that} \quad S_i/(I_i + N) \geq \gamma \quad \forall\ i \tag{3.1}$$

where vector $\mathbf{A}$ is

$$\mathbf{A} = \{A_0, A_1, ..., A_{M-1}\} \tag{3.2}$$

where A_i denotes the power of transmitter MS i, M denotes the number of MS pairs in the network, S_i denotes the power received at receiver MS i from its associated transmitter MS, I_i denotes the sum of received powers at receiver MS i from all non-associated transmitter MSs,

N denotes noise (Equation 2.8), and γ denotes the specified threshold SINR. Beam pointings are chosen such that the solution of Equation 3.1 is the minimum such solution. As stated in Section 1.2, the MS beamforming arrays are modeled as fixed patterns that can only be rotated, and not otherwise changed.

A closed form solution is not available, so a search is required. To facilitate the search, the search domain is quantized, i.e., MS pointings and transmitter MS powers are limited to discrete sets of values. The quantization scheme is as follows:

- Transmitter MS beams may point along LOS in azimuth toward their associated receiver MSs or may be scanned in azimuth over a discrete set of values. Beam pointing elevation is fixed.
- Receiver MS beams point along LOS toward their associated transmitter MSs, i.e., no attempt is made to optimize these pointings.
- Transmitter MS powers may be varied over a discrete set of values.

Specific values are provided and justified in Section 3.4.

As will be explained later, this quantization might result in none of the candidate solutions meeting all constraints. To overcome this, GAN selects the candidate solution that yields min(max(**A**)) from among the candidate solutions that meet the most constraints.

Another result of the quantization scheme is that multiple candidate solutions that meet the most constraints might yield the same min(max(**A**)). One way to overcome this problem is to search with finer quantization around each candidate solution. As will be shown later, this is also numerically intractable, so instead GAN selects from among the candidate solutions that meet the most constraints and yield the same min(max(**A**)) using the following *unconstrained* optimization:

$$\min(\max(\mathbf{D})) \tag{3.3}$$

where vector **D** is

$$\mathbf{D} = \{D_0, D_1, ..., D_{K-1}\} \tag{3.4}$$

where D_i denotes the power incident at DN position i, and K denotes the number of DN positions in the network.

Summarizing:

- GAN selects the candidate solution that meets the highest number of constraints.
- If multiple candidate solutions meet the highest number of (or, ideally, all) constraints, GAN selects the candidate solution that yields min(max($\mathbf{A}$)) from among those candidate solutions.
- If multiple candidate solutions meet the highest number of constraints and yield the same min(max($\mathbf{A}$)), GAN selects the candidate solution that yields min(max($\mathbf{D}$)) from among those candidate solutions.

3.3 Feasible Number of Candidate Solutions

The ideal quantization spans the space of all possible solutions to Equation 3.1. As will be demonstrated in this section, such a quantization scheme is intractable because of the resulting computational burden. Instead, we restrict the number of candidate solutions to make the brute-force search tractable. The feasible number of candidate solutions is calculated in this section.

Realization runtime t_R is

$$t_R = t_M \left[\left(\frac{R_\phi}{\Delta_\phi} + 1 \right) \left(\frac{R_A}{\Delta_A} + 1 \right) \right]^M \tag{3.5}$$

where t_M denotes the time required to evaluate a solution for a network with M MS pairs, referred to as "evaluation runtime;" R_ϕ and Δ_ϕ denote the transmitter MS pointing range and step size, respectively; R_A and Δ_A denote the A range and step size, respectively; and R_A and Δ_A are in decibels (dB). We assume the time required to evaluate solutions is much greater

than the time required to perform the other aspects of the simulation, so we neglect those other aspects.

Evaluation runtime t_M is estimated as follows. We created a program that performed a billion evaluations with the simulation parameters listed in Table 2.2. The program was written in C. The computer that ran this program was equipped with an Intel® Core™ i5 CPU at 1.6 GHz and 12 GB of RAM. The average t_M are presented in Table 3.1.

The ideal choice for R_ϕ is 360°. A suitable R_A is not obvious. However, R_A determines the range of distances between associated MSs for which received power can be held constant, i.e., R_A can be viewed as a limit on power control. Large R_A enables power control over a large range of distance between MSs. Path loss is proportional to distance squared (Equation 2.5), so $R_A = 30$ dB corresponds to the ability to keep power constant for distances varying over a ∼32:1 span (or rather, a ∼1 km:32 m span).

Step sizes Δ_ϕ and Δ_A should be fine enough to resolve solutions of the constrained optimization problem, but course enough to avoid solutions that are not significantly different. Transmitter MS pointing step size Δ_ϕ is defined relative to the MS antenna pattern. For example, $\Delta_\phi = \text{HPBW}/2 \sim 5°$ for the simulation parameters listed in Table 2.1, yielding 73 values. Transmitter MS power step size Δ_A of 1 dB yields 31 values. These ranges and step sizes would result in t_R of between an hour to multiple years for networks with three, five, and seven MS pairs. This precludes the desired 10,000 Monte Carlo realizations as in Chapter 2. Therefore, a coarser quantization scheme must be used to reduce the number of candidate solutions.

From Equation 3.5:

$$\left(\frac{R_\phi}{\Delta_\phi}+1\right)\left(\frac{R_A}{\Delta_A}+1\right)=\left(\frac{t_R}{t_M}\right)^{1/M} \tag{3.6}$$

where the term on the left is equal to the number of candidate solutions. We arbitrarily select 24 hours as the maximum reasonable simulation runtime. To perform 10,000 Monte Carlo realizations as in Chapter 2, the maximum reasonable t_R is 8.64 s. Therefore, the number of

Number of MS pairs M	**Evaluation runtime t_M**
3	∼400 ns
5	∼600 ns
7	∼800 ns

Table 3.1: Evaluation runtimes t_M for networks with varying M.

candidate solutions that can be accommodated are 278, 27, and 10 for networks with three, five, and seven MS pairs, respectively.

3.4 Feasible Quantization Scheme

The quantization scheme described in the previous section requires a greater number of candidate solutions than that which is feasible. A feasible quantization scheme is presented in this section. In the revised scheme, we restrict the range of angles for transmitter MS pointing and estimate (as opposed to search for) transmitter MS powers.

We consider twenty sets of candidate solutions. These sets are listed in Table 3.2. Each set has nine candidate pointings. Each candidate pointing is defined by its associated angle ϕ relative to the LOS pointing towards the associated receiver MS. Candidate pointings are uniformly spaced by Δ_ϕ. Transmitter MS pointing step sizes Δ_ϕ vary between sets by 0.5° and range from 0.5° to 10.0°. (Our justification for ignoring sets with $\Delta_\phi > 10.0°$ is explained in Section 3.5.) These sets are evaluated in Section 3.6.

In the revised scheme,transmitter MS power is not scanned, but rather is calculated. In PAN (as described in Section 2.2), transmitter MS power is set to meet a specified SNR threshold, i.e., interference is not considered when transmitter MS power is set. PAN sets transmitter MS power A as follows (repeating Equation 2.10):

$$A \leftarrow \frac{\rho N \alpha L}{G_T G_R} \quad \text{(PAN)}. \tag{3.7}$$

In GAN, Equation 3.7 is modified as follows. Power delivered to the receiver MS is lower when

the transmitter MS points away from LOS, because G_T is reduced. In GAN, a correction factor β is applied to increase A to compensate for the loss in G_T. The correction factor β for an associated pointing offset ϕ is

$$\beta(\phi) \leftarrow \frac{G_0}{G(\phi)} \tag{3.8}$$

where G_0 denotes broadside antenna gain (calculated with Equation 2.2) and $G(\phi)$ denotes antenna gain for angle ϕ (calculated with Equation 2.1). Thus GAN sets A as follows:

$$A \leftarrow \frac{\rho N \alpha \beta L}{G_T G_R} \quad \text{(GAN)}. \tag{3.9}$$

Summarizing the revised quantization scheme:

- Transmitter MS antennas point along one of the candidate pointings listed in Table 3.2. In Section 3.4, we will argue for $\Delta_\phi = 2.5^\circ$ (Set 5).
- Receiver MS antennas point along LOS toward their associated transmitter MSs, i.e., no attempt is made to optimize these pointings.
- Transmitter MS powers A are not optimized. Instead, A is set using Equation 3.9.

The revised quantization scheme requires evaluation of 9^M candidate solutions per realization. The resulting simulation runtime is ~ 10 hours for $M = 7$.

3.5 Selection of Pointing Step Size (Δ_ϕ)

To choose Δ_ϕ, we test the performance of GAN using the various possibilities listed in Table 3.2. To test the performance of GAN, we revisit the scenarios specified in Table 2.2. The SINR threshold γ (recall from Equation 3.1) is set to 6 dB.

CDFs of link SINR for some candidate solution sets are presented in Figures 3.1-3.3. For readability, the CDFs for only five sets from Table 3.2 are shown. The fractions of links that exhibit SINR < 6 dB are listed in Table 3.3. The same information is shown as a graph in Figure 3.4. Set 5 ($\Delta_\phi = 2.5°$) yielded the lowest fraction of links that exhibit SINR < 6 dB. Sets with $\Delta_\phi < 2.5°$ cover a span $< 20°$ ($= 2\cdot$HPBW), so presumably these underperform because the main lobe is not fully sampled. Sets with $\Delta_\phi > 2.5°$ presumably underperform because they do not sample the main lobe with sufficient resolution, and are essentially random samples from portions of the pattern outside of the main lobe.

CDFs of DN-position power for some candidate solution sets are presented in Figures 3.5-3.7. For readability, the CDFs for only five sets from Table 3.2 are shown. The plots are difficult to differentiate, but they seem to separate between approximately -140 dBm and -110 dBm. We arbitrarily choose the fractions of DN-position power < -130 dBm to compare the sets. The fractions of DN-position powers < -130 dBm are listed in Table 3.4. The same information is shown as a graph in Figure 3.8. We see that DN-position power using GAN tends to worsen with increasing Δ_ϕ, albeit slowly. This is probably due to higher transmitter MS powers associated with candidate solution sets with higher Δ_ϕ.

Thus, we choose to use the candidate solution set 5 with $\Delta_\phi = 2.5°$ to compare with PAN. This is justified because this set yielded the lowest fraction of links that exhibit SINR < 6 dB among the sets we evaluated, and we judge this to be more important than the minor improvement in DN-position power possible by going to smaller Δ_ϕ.

Set 1, $\Delta_\phi = 0.5°$		**Set 2**, $\Delta_\phi = 1.0°$		**Set 3**, $\Delta_\phi = 1.5°$		**Set 4**, $\Delta_\phi = 2.0°$	
ϕ	β	ϕ	β	ϕ	β	ϕ	β
0.0°	0.0 dB	0.0°	0.0 dB	0.0°	0.0 dB	0.0°	0.0 dB
±0.5°	0.1 dB	±1.0°	0.1 dB	±1.5°	0.2 dB	±2.0°	0.4 dB
±1.0°	0.1 dB	±2.0°	0.4 dB	±3.0°	1.0 dB	±4.0°	1.8 dB
±1.5°	0.2 dB	±3.0°	1.0 dB	±4.5°	2.3 dB	±6.0°	4.3 dB
±2.0°	0.4 dB	±4.0°	1.8 dB	±6.0°	4.3 dB	±8.0°	8.6 dB
Set 5, $\Delta_\phi = 2.5°$		**Set 6**, $\Delta_\phi = 3.0°$		**Set 7**, $\Delta_\phi = 3.5°$		**Set 8**, $\Delta_\phi = 4.0°$	
ϕ	β	ϕ	β	ϕ	β	ϕ	β
0.0°	0.0 dB	0.0°	0.0 dB	0.0°	0.0 dB	0.0°	0.0 dB
±2.5°	0.7 dB	±3.0°	1.0 dB	±3.5°	1.4 dB	±4.0°	1.8 dB
±5.0°	2.9 dB	±6.0°	4.3 dB	±7.0°	6.2 dB	±8.0°	8.6 dB
±7.5°	7.3 dB	±9.0°	11.8 dB	±10.5°	20.3 dB	±12.0°	28.4 dB
±10.0°	16.6 dB	±12.0°	28.4 dB	±14.0°	15.9 dB	±16.0°	13.4 dB
Set 9, $\Delta_\phi = 4.5°$		**Set 10**, $\Delta_\phi = 5.0°$		**Set 11**, $\Delta_\phi = 5.5°$		**Set 12**, $\Delta_\phi = 6.0°$	
ϕ	β	ϕ	β	ϕ	β	ϕ	β
0.0°	0.0 dB	0.0°	0.0 dB	0.0°	0.0 dB	0.0°	0.0 dB
±4.5°	2.3 dB	±5.0°	2.9 dB	±5.5°	3.6 dB	±6.0°	4.3 dB
±9.0°	11.8 dB	±10.0°	16.6 dB	±11.0°	26.4 dB	±12.0°	28.4 dB
±13.5°	17.3 dB	±15.0°	14.1 dB	±16.5°	13.3 dB	±18.0°	13.8 dB
±18.0°	13.8 dB	±20.0°	16.7 dB	±22.0°	23.6 dB	±24.0°	35.6 dB
Set 13, $\Delta_\phi = 6.5°$		**Set 14**, $\Delta_\phi = 7.0°$		**Set 15**, $\Delta_\phi = 7.5°$		**Set 16**, $\Delta_\phi = 8.0°$	
ϕ	β	ϕ	β	ϕ	β	ϕ	β
0.0°	0.0 dB	0.0°	0.0 dB	0.0°	0.0 dB	0.0°	0.0 dB
±6.5°	5.2 dB	±7.0°	6.2 dB	±7.5°	7.3 dB	±8.0°	8.6 dB
±13.0°	19.3 dB	±14.0°	15.9 dB	±15.0°	14.1 dB	±16.0°	13.4 dB
±19.5°	15.7 dB	±21.0°	19.3 dB	±22.5°	27.0 dB	±24.0°	35.6 dB
±26.0°	21.7 dB	±28.0°	18.4 dB	±30.0°	17.9 dB	±32.0°	19.4 dB
Set 17, $\Delta_\phi = 8.5°$		**Set 18**, $\Delta_\phi = 9.0°$		**Set 19**, $\Delta_\phi = 9.5°$		**Set 20**, $\Delta_\phi = 10.0°$	
ϕ	β	ϕ	β	ϕ	β	ϕ	β
0.0°	0.0 dB	0.0°	0.0 dB	0.0°	0.0 dB	0.0°	0.0 dB
±8.5°	10.0 dB	±9.0°	11.8 dB	±9.5°	13.9 dB	±10.0°	16.6 dB
±17.0°	13.3 dB	±18.0°	13.8 dB	±19.0°	14.9 dB	±20.0°	16.7 dB
±25.5°	23.3 dB	±27.0°	19.9 dB	±28.5°	18.1 dB	±30.0°	17.9 dB
±34.0°	23.3 dB	±36.0°	33.7 dB	±38.0°	32.0 dB	±40.0°	24.2 dB

Table 3.2: Candidate solution sets.

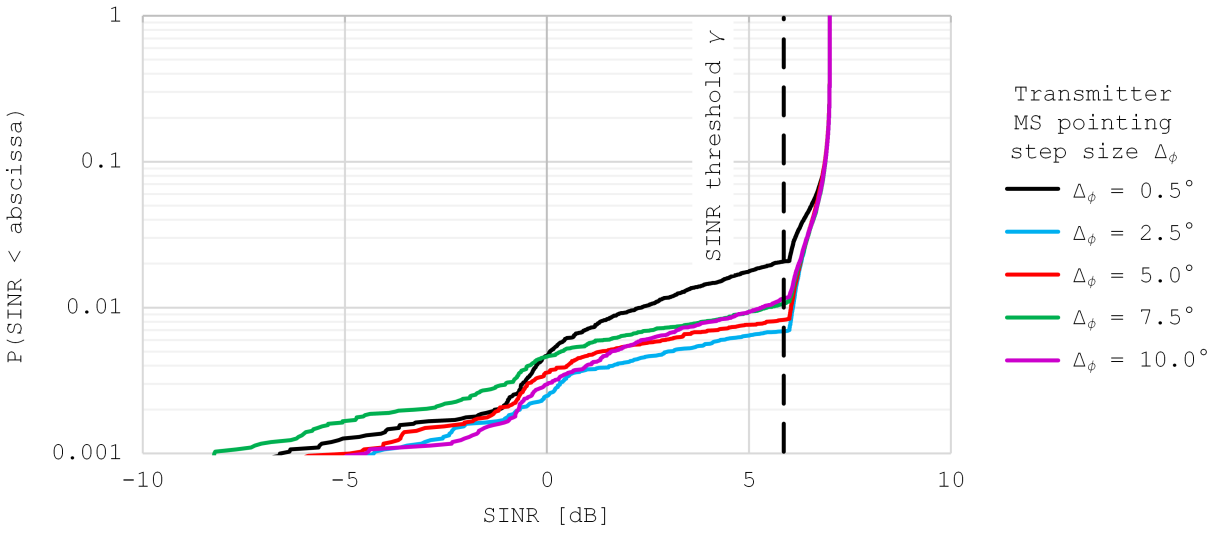

Figure 3.1: Comparing candidate solution sets listed in Table 3.2. CDFs of link SINR for GAN in null terrain with $M = 3$. For readability, CDFs for only five candidate solution sets are presented.

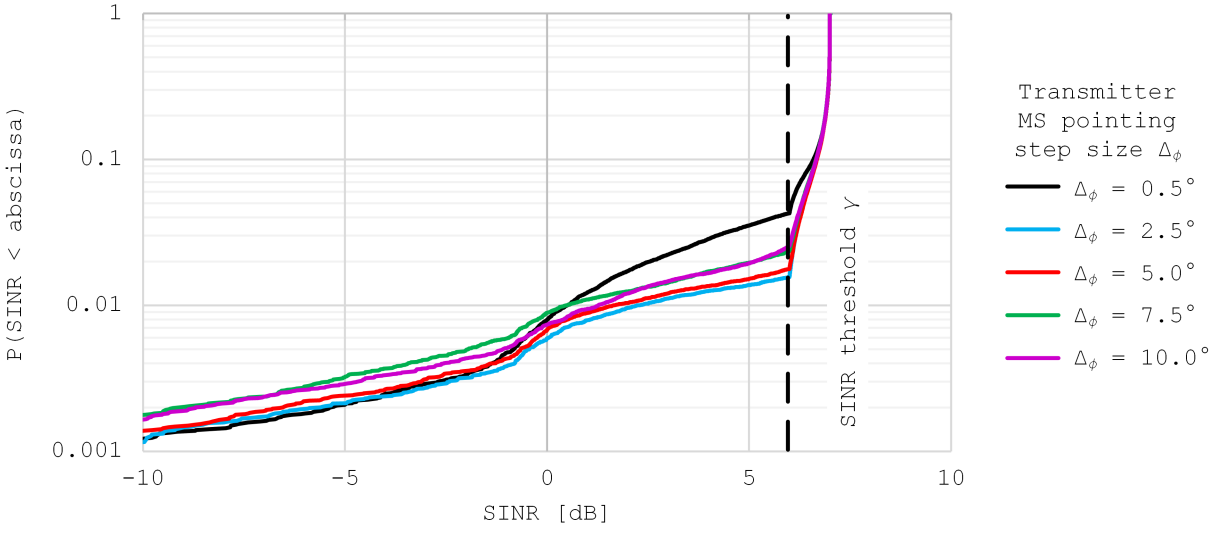

Figure 3.2: Same as Figure 3.1 except $M = 5$.

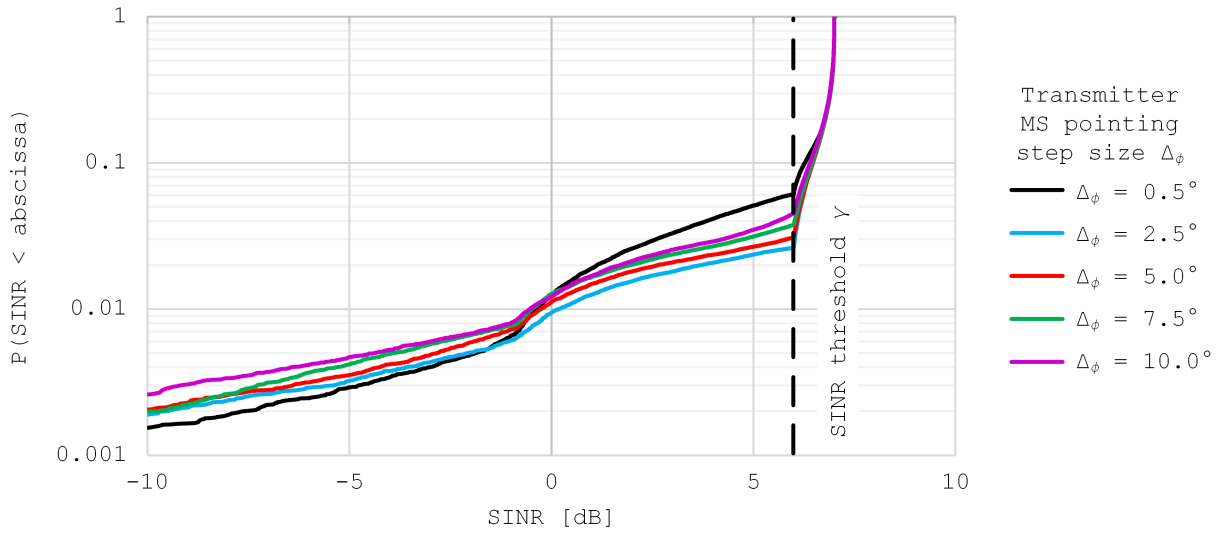

Figure 3.3: Same as Figures 3.1 and 3.2 except $M = 7$.

Candidate solution set	**Links that exhibit SINR** < 6 dB		
	$M = 3$	$M = 5$	$M = 7$
Set 1, $\Delta_\phi = 0.5°$	2.1%	4.3%	6.1%
Set 2, $\Delta_\phi = 1.0°$	1.4%	3.1%	4.4%
Set 3, $\Delta_\phi = 1.5°$	1.0%	2.2%	3.2%
Set 4, $\Delta_\phi = 2.0°$	0.8%	1.9%	2.8%
Set 5, $\Delta_\phi = 2.5°$	0.7%	1.6%	2.6%
Set 6, $\Delta_\phi = 3.0°$	0.8%	1.6%	2.8%
Set 7, $\Delta_\phi = 3.5°$	0.8%	1.7%	2.7%
Set 8, $\Delta_\phi = 4.0°$	0.9%	1.8%	3.2%
Set 9, $\Delta_\phi = 4.5°$	0.8%	1.8%	3.1%
Set 10, $\Delta_\phi = 5.0°$	0.8%	1.8%	3.1%
Set 11, $\Delta_\phi = 5.5°$	1.0%	2.4%	3.7%
Set 12, $\Delta_\phi = 6.0°$	1.4%	2.8%	4.3%
Set 13, $\Delta_\phi = 6.5°$	0.9%	2.2%	3.6%
Set 14, $\Delta_\phi = 7.0°$	1.0%	2.3%	3.8%
Set 15, $\Delta_\phi = 7.5°$	1.1%	2.4%	3.8%
Set 16, $\Delta_\phi = 8.0°$	1.1%	2.4%	4.2%
Set 17, $\Delta_\phi = 8.5°$	1.2%	2.7%	4.3%
Set 18, $\Delta_\phi = 9.0°$	1.1%	2.6%	4.5%
Set 19, $\Delta_\phi = 9.5°$	1.2%	2.8%	4.6%
Set 20, $\Delta_\phi = 10.0°$	1.2%	2.6%	4.5%

Table 3.3: Comparing candidate solution sets listed in Table 3.2. (GAN in null terrain.)

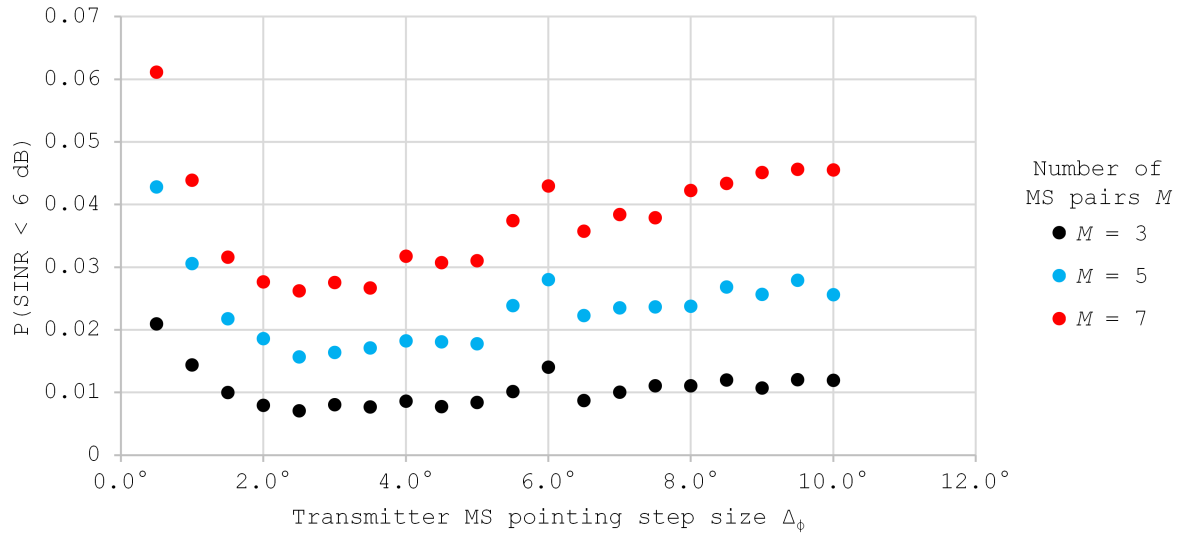

Figure 3.4: Table 3.3 presented graphically.

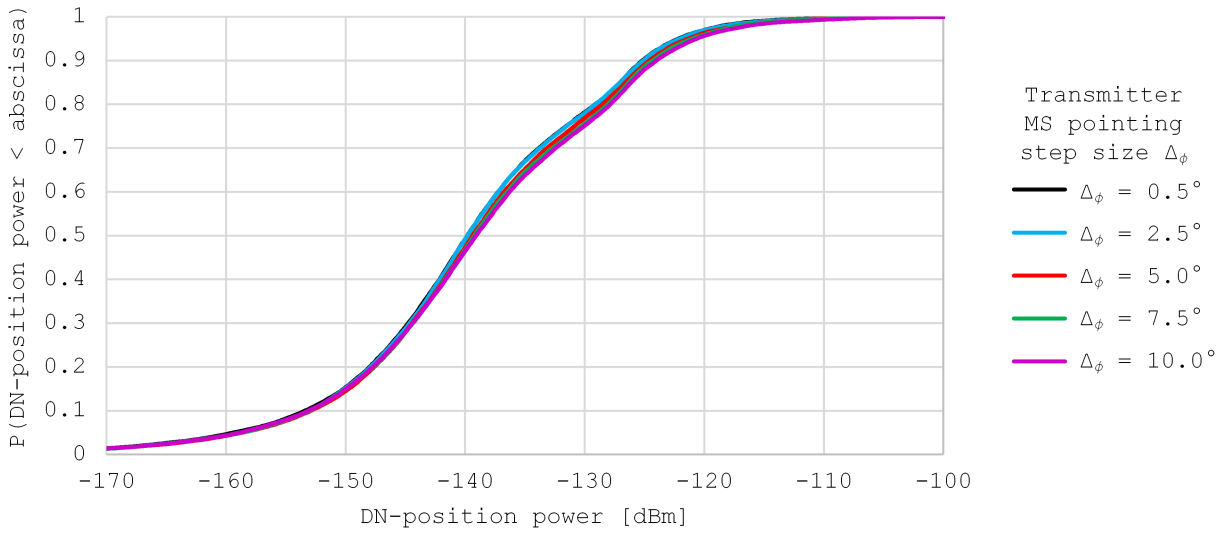

Figure 3.5: Comparing candidate solution sets listed in Table 3.2. CDFs of DN-position power for GAN in null terrain with $M = 3$. For readability, CDFs for only five candidate solution sets are presented.

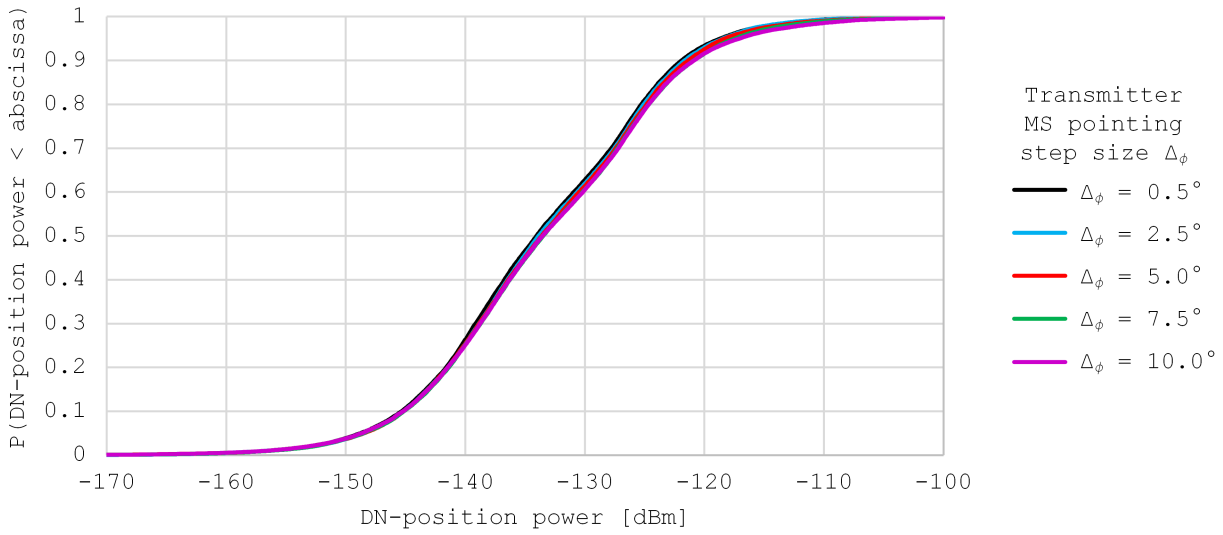

Figure 3.6: Same as Figure 3.5 except that $M = 5$.

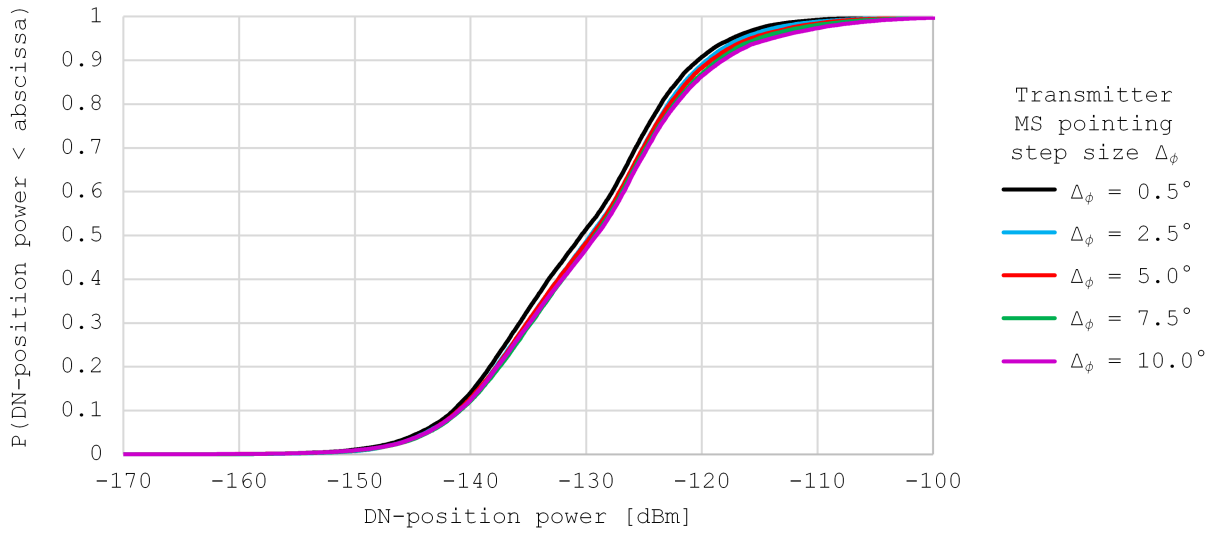

Figure 3.7: Same as Figures 3.5 and 3.6 except that $M = 7$.

Candidate solution set	DN-position powers < -130 dBm		
	$M = 3$	$M = 5$	$M = 7$
Set 1, $\Delta_\phi = 0.5°$	78.2%	62.8%	51.5%
Set 2, $\Delta_\phi = 1.0°$	79.0%	62.8%	50.3%
Set 3, $\Delta_\phi = 1.5°$	78.8%	62.2%	49.6%
Set 4, $\Delta_\phi = 2.0°$	78.2%	62.4%	49.9%
Set 5, $\Delta_\phi = 2.5°$	78.0%	61.9%	48.6%
Set 6, $\Delta_\phi = 3.0°$	77.7%	61.9%	49.6%
Set 7, $\Delta_\phi = 3.5°$	77.4%	61.8%	48.7%
Set 8, $\Delta_\phi = 4.0°$	77.1%	62.1%	49.1%
Set 9, $\Delta_\phi = 4.5°$	77.5%	60.7%	48.8%
Set 10, $\Delta_\phi = 5.0°$	76.9%	61.4%	48.4%
Set 11, $\Delta_\phi = 5.5°$	77.1%	62.2%	49.1%
Set 12, $\Delta_\phi = 6.0°$	76.5%	62.2%	49.1%
Set 13, $\Delta_\phi = 6.5°$	76.4%	61.0%	47.6%
Set 14, $\Delta_\phi = 7.0°$	77.0%	61.1%	47.7%
Set 15, $\Delta_\phi = 7.5°$	75.6%	60.6%	47.0%
Set 16, $\Delta_\phi = 8.0°$	76.1%	61.2%	48.1%
Set 17, $\Delta_\phi = 8.5°$	75.8%	60.6%	47.2%
Set 18, $\Delta_\phi = 9.0°$	75.4%	60.5%	47.1%
Set 19, $\Delta_\phi = 9.5°$	75.1%	59.9%	46.2%
Set 20, $\Delta_\phi = 10.0°$	75.1%	60.5%	46.9%

Table 3.4: Comparing candidate solution sets listed in Table 3.2. Fractions of DN-position powers < -130 dBm for GAN in null terrain.

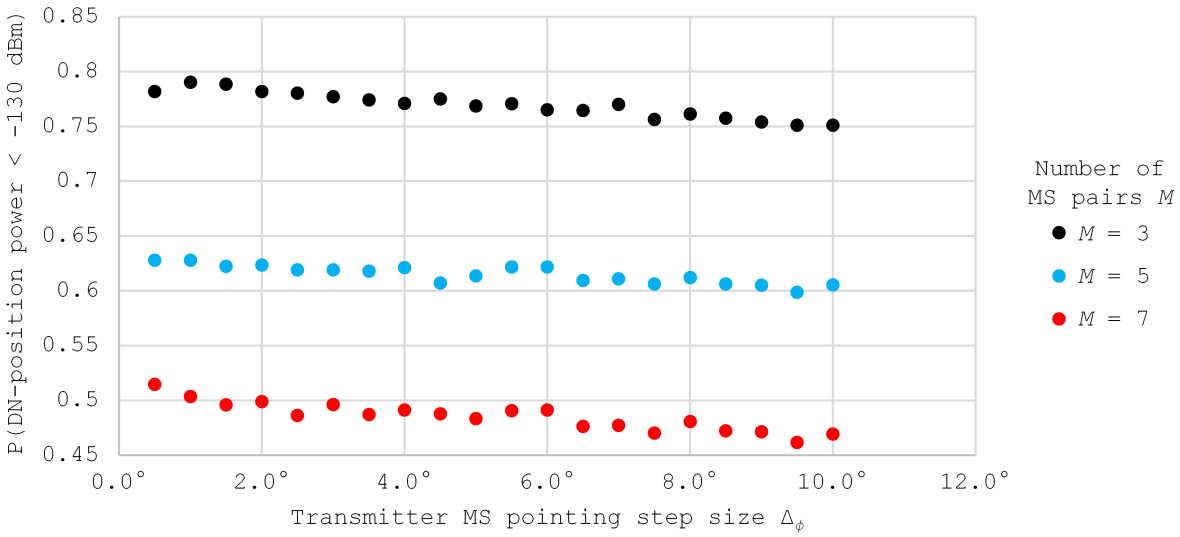

Figure 3.8: Table 3.4 presented graphically.

3.6 Results

CDFs of link SINR for GAN in null terrain are presented in Figure 3.9. CDFs for PAN in null terrain are included for comparison (repeated from Figure 2.6). The fractions of links that exhibit SINR < 6 dB are listed in Table 3.5. As expected, GAN yields significant performance gains over PAN. GAN decreases the fractions of links that exhibit SINR < 6 dB relative to PAN by 2.1%, 4.2%, and 5.8% for networks with three, five, and seven MS pairs, respectively. However, GAN has greater fractions of links that exhibit SINR < -4 dB relative to PAN for networks with three and five MS pairs. This is likely due to GAN degrading links that cannot exhibit SINR ≥ 6 dB to minimize $\mathbf{A}$. However, the number of affected links is much less than the number of links improved.

The fractions of realization where GAN finds multiple solutions and thus "falls back" to the unconstrained optimization problem (Equation 3.3) are listed in Table 3.6. These fractions are greater than 99.7% for networks with three, five, and seven MS pairs. This suggests that the quantization scheme limits the extent to which the solution can be optimized.

The average t_R from the simulations of GAN in null terrain are listed in Table 3.7. For comparison, the average t_R from the simulations of PAN in null terrain are included. The uncertainty of these measurements is ~ 1 ms. As expected, the difference between PAN t_R and GAN t_R increases with increasing M. This is due to exponentially increasing number of calculations required for GAN in networks with increasing M. The observed computational burden of GAN seems to be quite close to the values predicted.

CDFs of DN-position power for GAN in null terrain are presented in Figure 3.10. CDFs for PAN in null terrain are included for comparison (repeated from Figure 2.7). It is apparent that the benefit of GAN over PAN in reducing DN-position power is small at best and decreases with M.

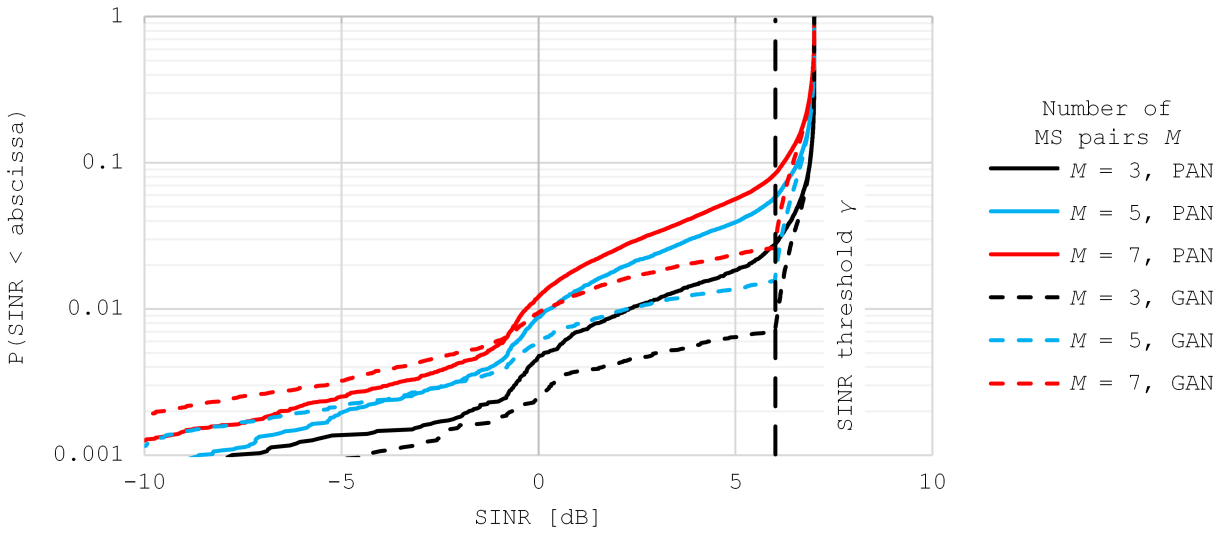

Figure 3.9: CDFs of link SINR for PAN and GAN in null terrain.

Number of MS pairs M	**Links that exhibit SINR** < 6 **dB**		
	PAN	GAN	Difference
3	2.8%	0.7%	-2.1%
5	5.8%	1.6%	-4.2%
7	8.4%	2.6%	-5.8%

Table 3.5: Fractions of links that exhibit SINR < 6 dB for PAN and GAN in null terrain.

Number of MS pairs M	**Realizations where GAN falls back to Equation** 3.3
3	97.8%
5	99.9%
7	100.0%

Table 3.6: Fractions of realizations where GAN "falls back" on Equation 3.3.

Number of MS pairs M	**Realization runtimes** t_R		
	PAN	GAN	Equation 3.5
3	< 1 ms	< 1 ms	~ 292 μs
5	< 1 ms	~ 36 ms	~ 35 ms
7	< 1 ms	$\sim 2,422$ ms	$\sim 3,827$ ms

Table 3.7: Realization runtimes t_R for PAN and GAN in null terrain. Predicted t_R for GAN are calculated with Equation 3.5.

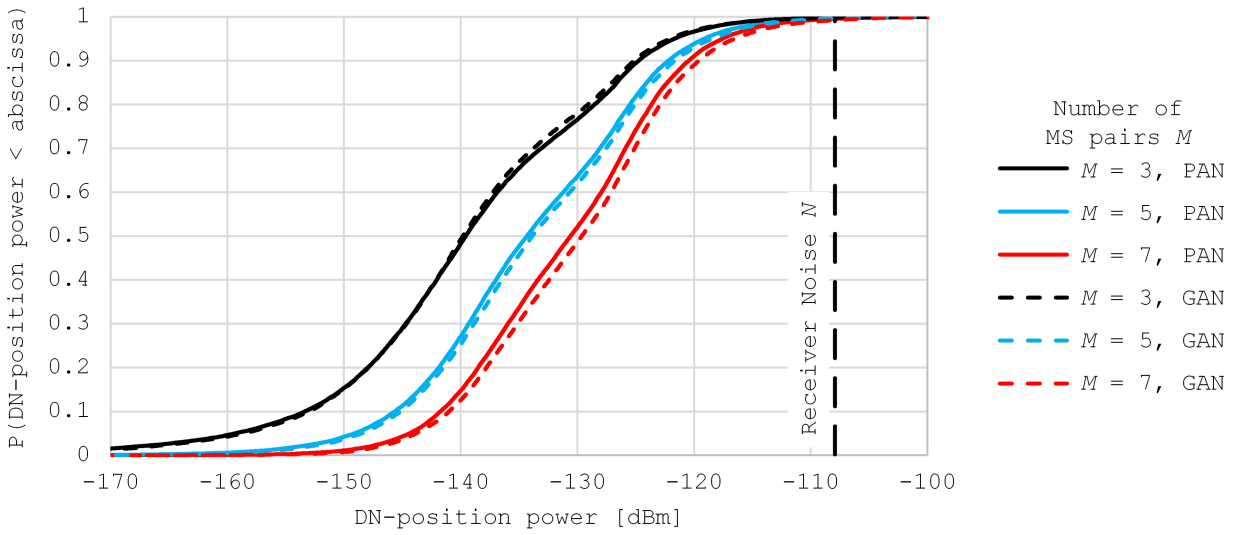

Figure 3.10: CDFs of DN-position power for PAN and GAN in null terrain.

3.7 Conclusions

The efficacy of coordinated beamforming in null terrain using GAN has been demonstrated. It was determined that GAN can decrease the fractions of links that exhibit SINR < 6 dB by 2.1%, 4.5%, and 5.8% relative to the non-coordinated beamforming scheme PAN for networks with three, five, and seven MS pairs, respectively, as shown in Figure 3.9 and listed in Table 3.5. However, GAN does not significantly improve DN-position power relative to PAN, as shown in Figure 3.10.

So far, only networks in null terrain have been considered. Terrestrial networks will likely be in environments with obstructions that affect wave propagation. In the next chapter, we present a propagation model for such environments, which will be employed in Chapter 5 to evaluate PAN and other coordinated beamforming schemes.

Chapter 4

Millimeter Wave Propagation in Presence of Obstructions

In Chapters 2 and 3, networks were simulated in null terrain (as defined in Section 1.2). Terrestrial networks operate in environments with obstructions that affect wave propagation. The propagation models commonly used for network optimization are statistical, see e.g. [9]. However, the propagation model presented in this thesis is deterministic. The reason for this is that the work presented in this thesis supports future work on terrain discovery, as will be explained in Section 6.3. In this chapter, a deterministic propagation model for millimeter wave networks in environments with obstructions is presented. This chapter concludes with a demonstration of the propagation model which will be used in later chapters.

This chapter is organized as follows. The propagation model is presented in Section 4.1. The demonstration of the propagation model is presented in Section 4.2. A convenient method of classifying links based on path availability is presented in Section 4.2, as well.

4.1 Propagation Model

An example of wave propagation in an environment with obstructions is shown in Figure 4.1. Wave propagation in the presence of obstructions can be described in terms of the following propagation mechanisms: reflection, diffraction, and propagation through obstructions. To simplify our model, we exclude propagation through obstructions and diffraction. This is justified because diffraction tends to dominate over propagation through obstructions, and reflection tends to dominate over diffraction, see e.g. [1, 10, 11]. Thus, we get a reasonable estimate by considering only line-of-sight (LOS) propagation and reflection.

Since we only consider LOS propagation and reflection, we use geometrical optics (GO) to model wave propagation. In GO, waves propagate in straight line paths, referred to as "rays." Rays that intersect obstructions are reflected. The direction of a reflected ray can be determined using Snell's law. (For more on GO, see e.g., [4, Section 16.1].)

In principle, rays can be reflected any number of times. However, tracking multiply-reflected paths is computationally intensive. Instead, we shall terminate rays at the second point of reflection. This is justified because path length d for multiply-reflected paths is always greater than d for LOS and singly-reflected paths, typically resulting in orders of magnitude additional path loss.

A general expression for electric field E at a receiver is

$$E = \frac{E_0 e^{-jk_0 d_0}}{d_0} + \sum_{i=1}^{n_r} \frac{R_i E_i e^{-jk_i d_i}}{d_i} \tag{4.1}$$

where E_0 denotes an arbitrary constant representing the magnitude and phase of the source; subscript 0 denotes the LOS path; k denotes wavenumber $(2\pi/\lambda)$; n_r denotes the number of reflected-ray paths; E_i denotes electric field at a point of reflection; R_i denotes reflection coefficient, which is the ratio of reflected electric field intensity to the incident electric field intensity at the point of reflection; and d_i denotes the total distance of a reflected-ray path. We assume that all MS antennas in the network are vertically polarized.

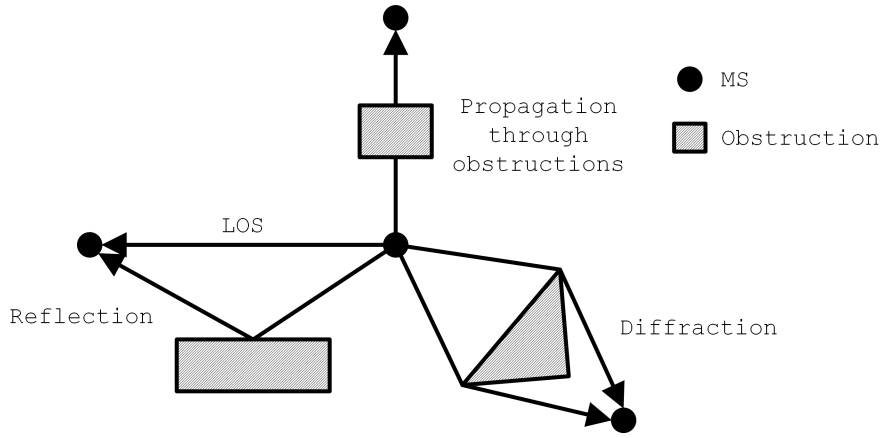

Figure 4.1: Propagation mechanisms.

Before proceeding, we should consider whether reflection is well-modeled as that associated with a perfectly smooth flat surface, or whether diffuse scattering due to surface roughness must be considered. An illustration of surface roughness is presented in Figure 4.2. A reflection is diffuse when the surface from which it reflects fails the Rayleigh criterion:

$$[\max(h_s) - \min(h_s)] < \frac{\lambda}{8\cos\theta_i} \tag{4.2}$$

where h_s denotes the function for surface roughness height, and θ_i denotes angle of incidence (where normal incidence is $\theta_i = 0°$). For a derivation, see e.g. [5, Section 3.3]. The frequency in Chapters 2 and 3 was 30 GHz. The Rayleigh criterion for 30 GHz and varying θ_i is shown in Figure 4.3. For surfaces with $[\max(h_s) - \min(h_s)] \leq 1.25$ mm, diffuse scattering is negligible, thus R is approximately equal to the specular reflection coefficient. For surfaces with $[\max(h_s) - \min(h_s)] > 1.25$ mm, diffuse scattering might be non-negligible, and so R should be calculated as the product of the specular reflection coefficient and a diffuse scattering factor f_s:

$$f_s(\sigma_s) = \exp\left[-\frac{1}{2}\left(\frac{4\pi\sigma_s\cos\theta_i}{\lambda}\right)^2\right] \tag{4.3}$$

where scalar σ_s is the standard deviation of h_s; for more on this formula, see e.g. [5, Section 3.3].

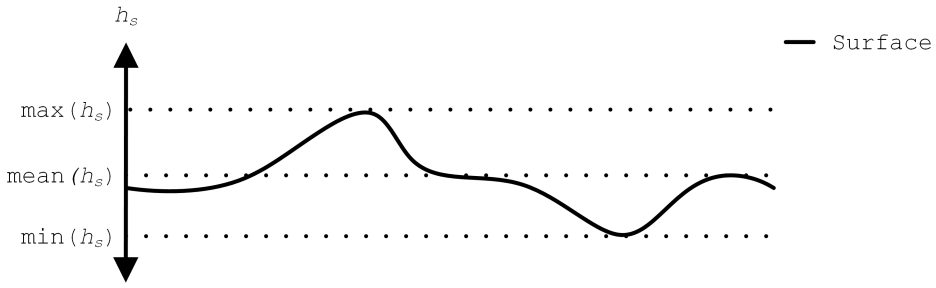

Figure 4.2: Illustration of surface roughness.

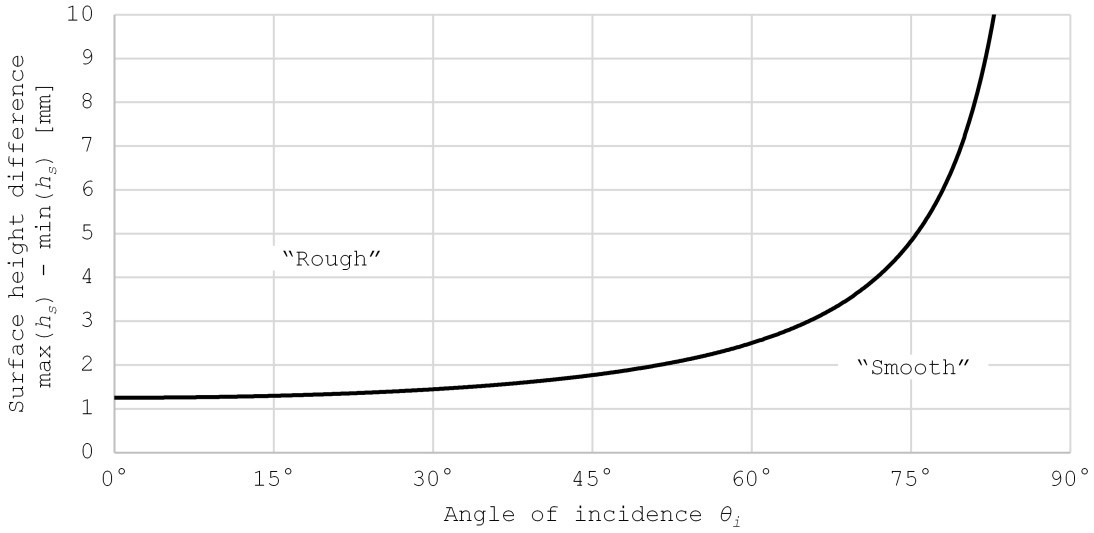

Figure 4.3: Rayleigh criterion for 30 GHz for varying θ_i.

To get a rough idea of what to expect, let us assume

$$\max(h_s) \approx \text{mean}(h_s) + 3\sigma_s \tag{4.4}$$

$$\min(h_s) \approx \text{mean}(h_s) - 3\sigma_s. \tag{4.5}$$

Subsequently, $\sigma_s = [\max(h_s) - \min(h_s)]/6$. The diffuse scattering factor f_s for 30 GHz and varying θ_i is shown in Figure 4.4. Note that f_s can be significantly less than 1 for $[\max(h_s) - \min(h_s)] > 1$ mm.

Because power loss due to reflection is proportional to $|R|^{-2}$, power loss due to diffuse scattering is proportional to f_s^{-2}. For θ_i near broadside, we see that power loss due to diffuse

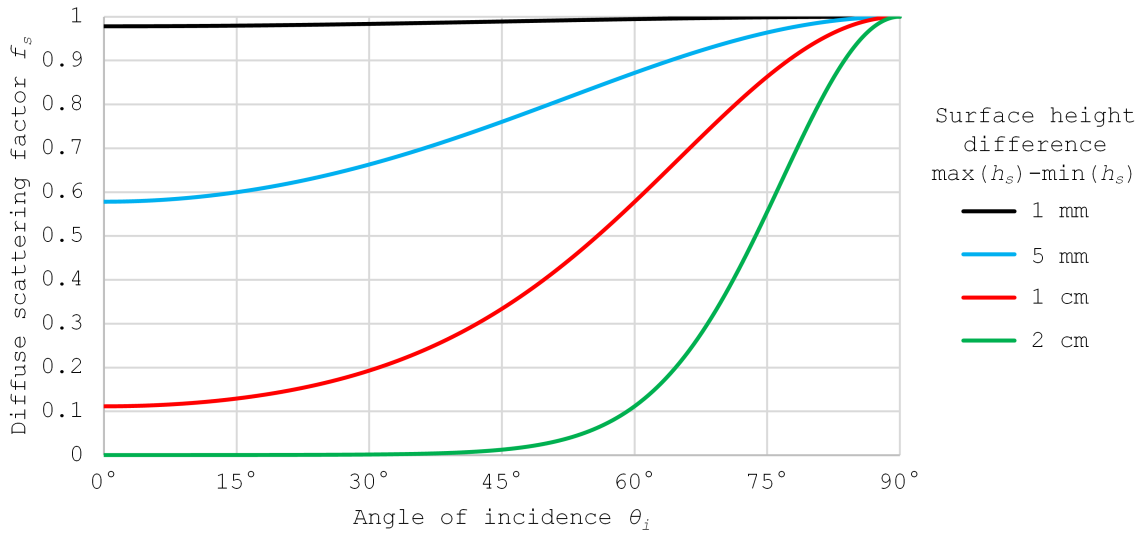

Figure 4.4: Diffuse scattering factor f_s for 30 GHz with $\sigma_s = [\max(h_s) - \min(h_s)]/6$ and varying θ_i.

scattering can be significant when the Rayleigh criterion is exceeded. Nevertheless, we shall assume $f_s = 1$ going forward in order to simplify simulations. This is justified as follows:

- The magnitude of the specular reflection coefficient decreases with decreasing θ_i (see Figure 4.5), so reflections for which f_s is smallest will already be weaker.
- From the Friis transmission formula, path loss L is (repeating Equation 2.4):

$$L = \left(\frac{4\pi d}{\lambda}\right)^n \tag{4.6}$$

  where n varies with propagation model. As described in Section 2.1, we restrict $d \ll d_b$, so that n can be assumed to be about 2. In our simulations, paths are never less than 1 m and never greater than 1 km. Thus, L varies by ~ 60 dB. In contrast, f_s varies between 0.1 and 1 for $[\max(h_s) - \min(h_s)] \leq 1$ cm, corresponding to 20 dB variation in received power. Thus, even when f_s variation is significant, it is small relative to the variation in L.

On this basis, we set $f_s = 1$. This can be interpreted as either ignoring surface roughness, i.e., assuming perfectly smooth reflecting surfaces; or as a reasonable approximation for the

purposes of gathering link statistics, although not for deterministic link-by-link prediction.

Since we assume that $f_s = 1$, R is approximately equal to the specular reflection coefficient. The specular reflection coefficient is calculated with the Fresnel reflection coefficients. Since we assume all antennas in our simulation are vertically polarized, R is the Fresnel reflection coefficient for perpendicular polarization relative to the plane of incidence (i.e., parallel to the reflecting surface):

$$R = \frac{\cos\theta_i - \sqrt{\epsilon_r - \sin^2\theta_i}}{\cos\theta_i + \sqrt{\epsilon_r - \sin^2\theta_i}} \tag{4.7}$$

where ϵ_r denotes the relative permittivity of the obstruction material; for a derivation, see e.g. [5, Section 3.2.1]. Zhekov, Franek, and Penderson (2020) measured ϵ_r for outdoor materials at millimeter waves [12]. The magnitude of the R for some representative materials at 30 GHz is shown in Figure 4.5. Note that $|R|$ is never less than ~ 0.25, and increases with θ_i. With this in mind, we approximate $|R| = 1$ in order to simplify our calculations. This is justified because power loss associated with reflections will be negligible relative to L. Power loss associated with reflections is proportional to $|R|^{-2}$, so this power loss < 6 dB. In contrast, path loss $L \geq 42$ dB (i.e., $L \sim 42$ dB for the shortest path distance 1 m). So considering that surface roughness has only a relatively minor effect and also specular reflection is expected to be relatively efficient, we assume unity R going forward.

Rays that travel along different paths arrive at the receiver position with different phases, causing multipath interference. To simplify calculations, total received power is calculated as the sum of the powers of the individual rays, i.e., incoherent addition of power is assumed. Justification can be found in e.g. [6, Section 8.4].

We use different methods to determine LOS and reflected-ray paths. To determine if the LOS path between positions is unblocked, we generate a ray along the LOS path and determine if the ray intersects any obstructions between the positions. We use the shooting and bouncing ray method (SBR) to determine reflected-ray paths. For more on the SBR method, see e.g. [13]. An illustration of the SBR method is shown in Figure 4.6. Rays need be launched only about the azimuth axis because all MS antennas are placed at the same height above ground and beams point parallel to ground. Rays are launched from the transmitter MS over

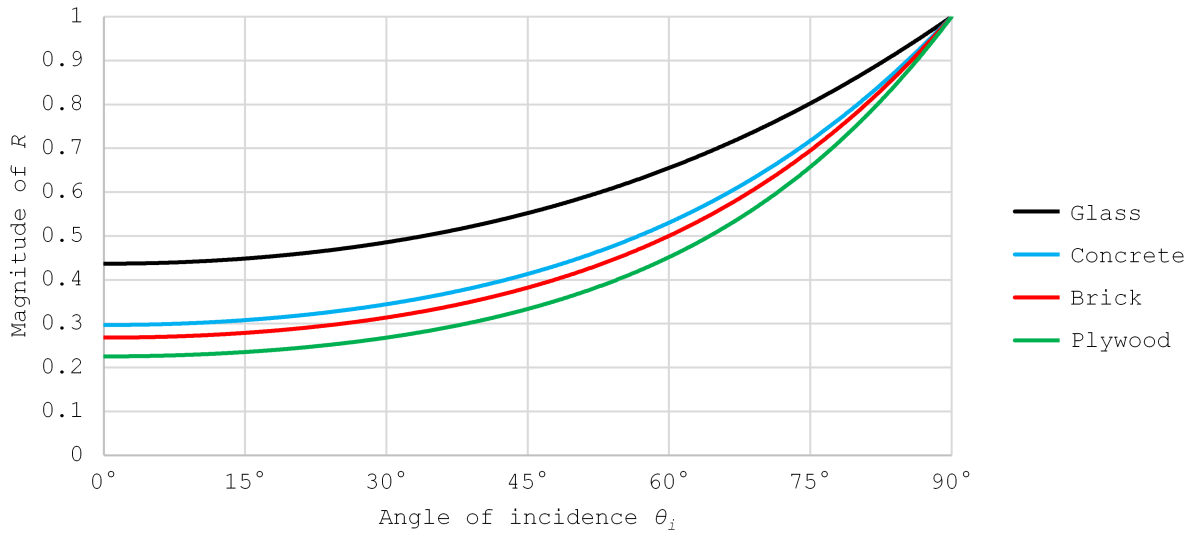

Figure 4.5: Magnitude of R for some representative materials at 30 GHz for varying θ_i.

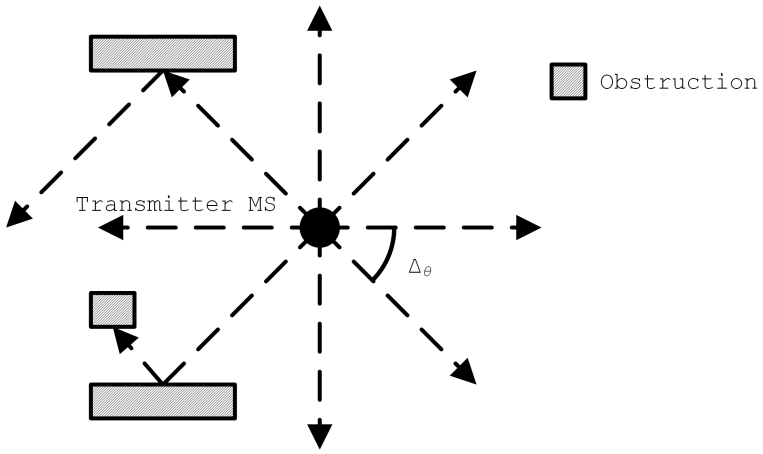

Figure 4.6: The SBR method.

a range of 360° in azimuth with a specified angular spacing Δ_θ. We arbitrarily select $\Delta_\theta = 1°$. Rays that intersect obstructions are reflected. Reflected rays that intersect a second obstruction are terminated at the point of the second reflection.

Using this procedure, receiver positions are likely not to be precisely intersected by reflected rays. The following method is used to determine if a reflected ray should be considered received at a receiver position. An illustration of the method is shown in Figure 4.7. Position Q is the position along a reflected ray that is closest to a receiver position. A reflected ray is considered received if the distance between the receiver position and position Q is less than

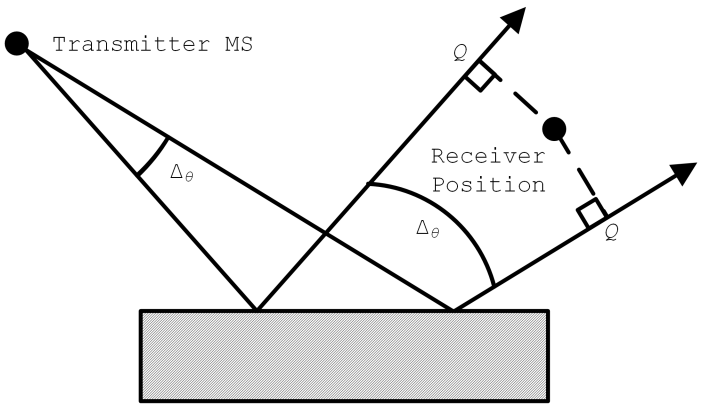

Figure 4.7: Illustration of method used to determine if a reflected ray is considered received at a receiver position.

distance threshold d_T. Distance threshold d_T is calculated as follows:

$$d_T \leftarrow d_Q \tan\left(\frac{\Delta_\theta}{2}\right) \tag{4.8}$$

where d_Q is the distance between the transmitter MS and position Q along the reflected-ray path. If two adjacent rays meet this criterion, only the ray with the smallest distance between the receiver position and its associated Q is considered received.

4.2 Propagation Model Demonstration; Path Classification

To demonstrate the propagation model, we examine the scenario shown in Figure 4.8. This terrain is defined in the Appendix. A transmitter MS equipped with an omnidirectional antenna is placed at the center of a circular track with a radius of 500 m. LOS and reflected-ray paths between the transmitter MS and positions along the track are shown in Figures 4.9 and 4.10.

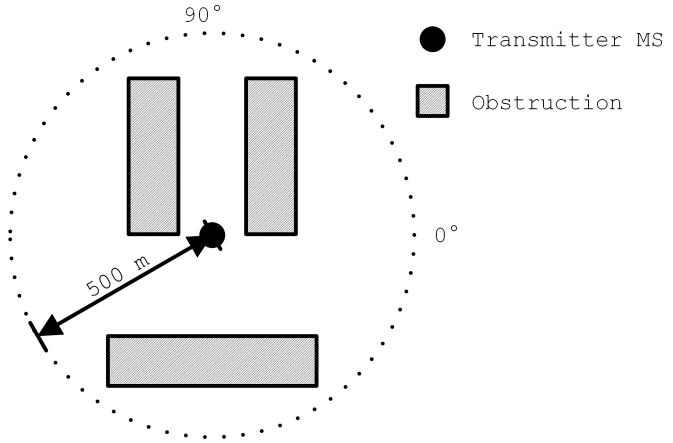

Figure 4.8: Scenario used to demonstrate propagation model.

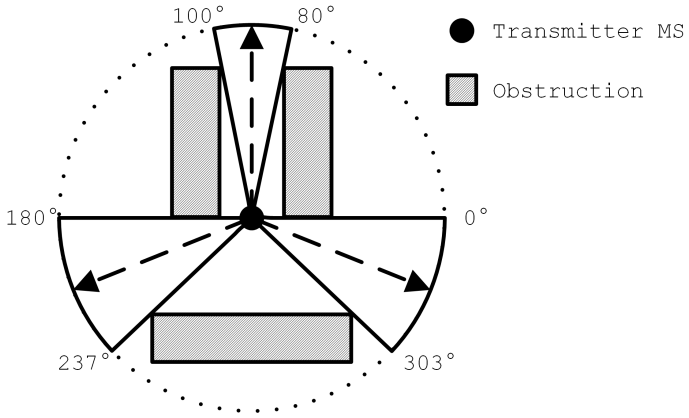

Figure 4.9: Zones in which LOS paths exist.

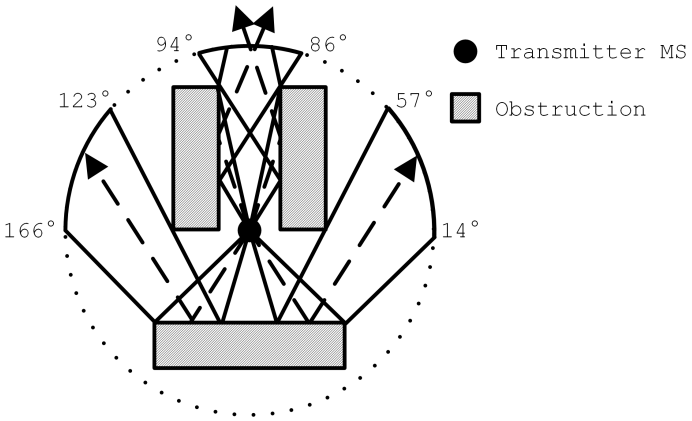

Figure 4.10: Zones in which reflected-ray paths exist.

We classify pairs of positions into four cases:

- Case I: The LOS path is blocked and no reflected-ray paths exist, e.g., 270° in Figures 4.8-4.10. Links between Case I MS pairs are referred to as "futile links" because link SINR = 0 regardless of MS pointing and transmitter MS power. Ideally, MS pairs with futile links should not transmit in order to avoid emitting unnecessary interference to non-futile links.
- Case II: The LOS path is unblocked and no reflected-ray paths exist, e.g., 200° in Figures 4.8-4.10.
- Case III: The LOS path is blocked but one or more reflected-ray paths exist, e.g., 45° in Figures 4.8-4.10.
- Case IV: The LOS path is unblocked and one or more reflected-ray paths exist, e.g., 90° in Figures 4.8-4.10.

This classification will prove useful in the analysis of simulation results in Chapter 5.

Received power at 30 GHz between the transmitter MS and positions along the track is calculated and presented in Figure 4.11. Received power P_R is calculated with the Friis transmission formula (repeating Equation 2.4):

$$P_R = AG_TG_RL^{-1} \tag{4.9}$$

where A denotes transmitter MS power, and G_T and G_R denote transmitter and receiver antenna gain. For simplicity, $G_R \leftarrow 0$ dBi and $A \leftarrow 0$ dBm. Since the transmitter MS is equipped with an omnidirectional antenna, $G_T = 0$ dBi. Again, powers received along different paths are summed, as explained in Section 4.1.

In the next chapter, the propagation model and classification scheme defined in this chapter will be used to evaluate PAN and other schemes in terrain with obstructions.

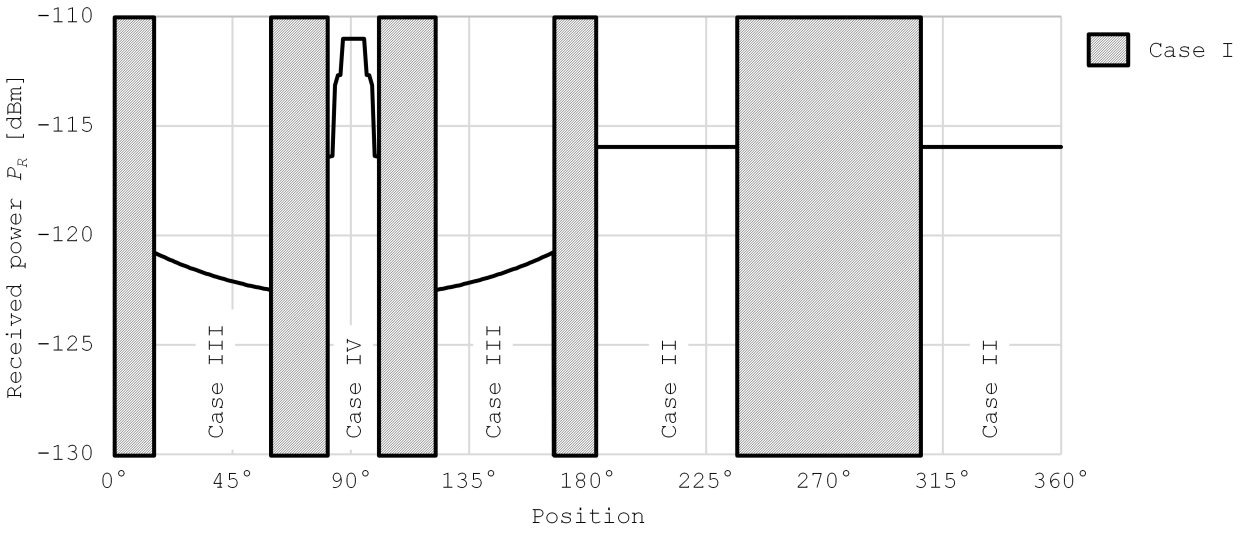

Figure 4.11: Received power P_R at positions along circular track shown in Figure 4.8.

Chapter 5

Pairwise and Global Schemes in Residential Terrain

In Chapters 2 and 3, networks were simulated in null terrain (as defined in Section 1.2). In Chapter 4, a propagation model for terrain with obstructions was presented. In this chapter, schemes using knowledge of the terrain are presented. The terrain used in this chapter is referred to as "residential terrain" and is described in Section 5.1.

This chapter is organized as follows. To establish a baseline of performance for the schemes with knowledge of the terrain, we simulate the Pairwise Assuming Null terrain (PAN) in residential terrain. Results are presented in Section 5.1. A pairwise scheme with perfect knowledge of the terrain (PPK) is presented in Section 5.2. A global scheme with perfect knowledge of the terrain (GPK) is presented in Section 5.3. Conclusions are presented in Section 5.4.

5.1 PAN in Residential Terrain

Residential terrain is shown in Figure 5.1. This terrain geometry is defined in the Appendix. MSs are restricted to positions along the track shown in Figure 5.1. The simulation parameters

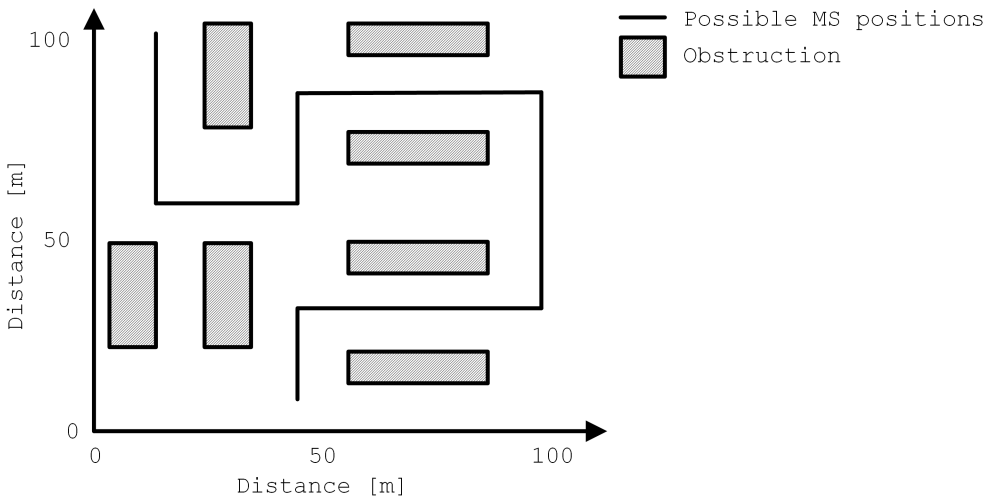

Figure 5.1: Residential terrain.

for this chapter are listed in Table 5.1. The fractions of MS pairs in each path-availability case (as described in Section 4.2) are presented in Table 5.2.

CDFs of link SINR are presented in Figure 5.2. For comparison, the CDFs of link SINR for PAN in null terrain (from Figure 2.6) are included. As expected, the performance of PAN in non-null terrain is catastrophic. This is due to the large fraction (53.5%) of links for which there is no LOS path. The fractions of links that exhibit SINR < 6 dB are listed in Table 5.3. Note that the differences in fractions that exhibit SINR < 6 dB between PAN in null terrain and residential terrain are approximately equal to the fraction of links where the LOS path is blocked (Cases I and III).

CDFs of DN-position power are presented in Figure 5.3. DN-position powers are lower in residential terrain than in null terrain. This is due to obstructions blocking paths between transmitter MSs and DN positions for networks in residential terrain. This effect decreases as M increases because the number of unblocked paths between transmitter MSs and DN positions increases with increasing M.

Terrain	Residential Terrain
MS positions	Random placement along track shown in Figure 5.1
# of MS pairs M	3, 5, 7
# of DN positions	3 randomly placed
# of realizations	10,000

Table 5.1: Simulation parameters for networks in residential terrain.

	LOS path blocked	**LOS path unblocked**
No reflected-ray paths exist	37.5% (Case I)	14.2% (Case II)
One or more reflected-ray paths exist	16.0% (Case III)	32.3% (Case IV)

Table 5.2: Fractions of MS pairs in each path-availability case for networks in residential terrain.

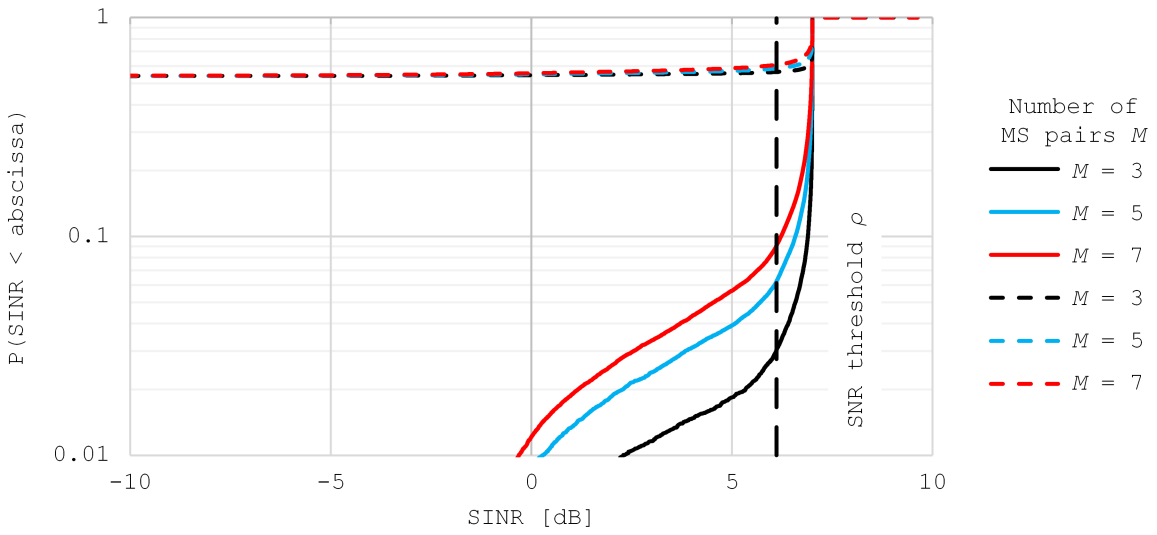

Figure 5.2: CDFs of link SINR for PAN in null (solid lines) and residential (dashed lines) terrain.

Number of MS pairs M	**Links that exhibit SINR < 6 dB**		
	Null terrain	Residential terrain	Difference
3	2.8%	56.3%	53.6%
5	5.8%	58.3%	52.6%
7	8.4%	60.5%	52.1%

Table 5.3: Fractions of links that exhibit SINR < 6 dB for PAN in null and residential terrain.

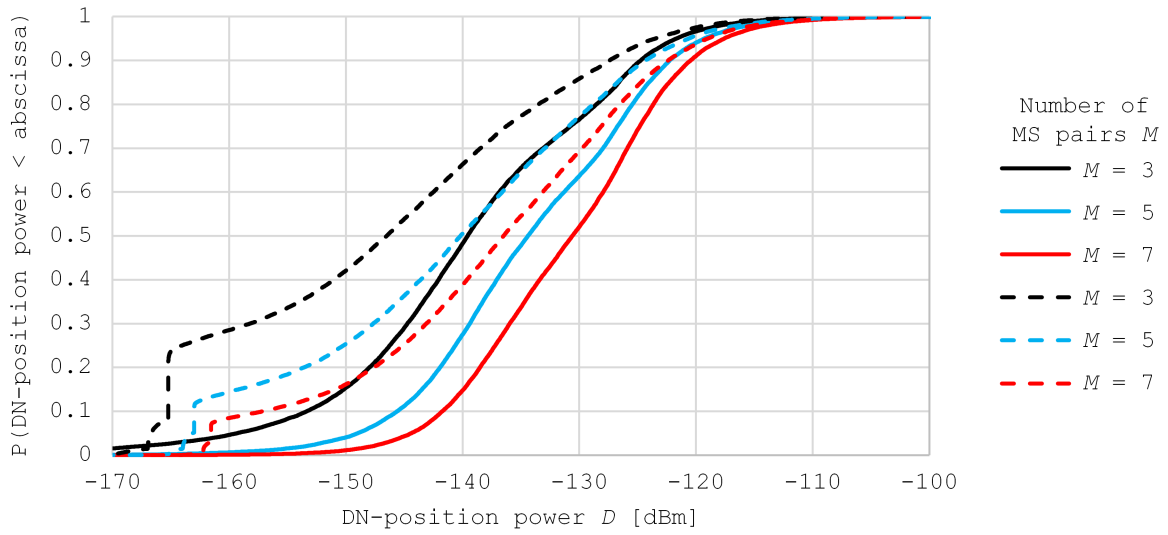

Figure 5.3: CDFs of DN-position power for PAN in null terrain (solid lines) and residential (dashed lines) terrain.

5.2 PPK in Residential Terrain

The pairwise scheme presented in this section is referred to as the "Pairwise assuming Perfect Knowledge of terrain" (PPK) scheme. PPK sets pointings and powers as follows:

- For Case I (futile), no attempt is made to create a link, i.e., transmitter MS power $A \leftarrow 0$ so as to not create interference for non-futile links.

- For Cases II and IV (LOS path unblocked), both transmit and receive beams point along the LOS path toward their associated MS. As in PAN, A is set to make the receiver MS's SNR equal to ρ. For Case IV, multiple paths exist between paired MSs. Received power from all available paths could be considered when setting A to minimize A. However, only received power from the LOS path is considered in this calculation. This is justified in Section 5.3. Thus, A is set as follows (repeating Equation 2.10):

$$A \leftarrow \frac{\rho N \alpha L}{G_T G_R}. \tag{5.1}$$

- For Case III (LOS path blocked, reflected-ray path exists), PPK points both transmit and receive beams along a reflected-ray path, i.e., beams point toward the point of reflection

associated with a reflected-ray path. If multiple reflected-ray paths exist, PPK points beams along the path with the smallest length d. Transmitter MS power A is set using Equation 5.1 where L is calculated using the length of this path. Analogous to how A is set for Case II and IV MS pairs, only received power from the shortest reflected-ray path is considered in this calculation.

To demonstrate the performance of PPK, we repeat the experiment in Section 5.1 with PPK. CDFs of non-futile link SINR are presented in Figure 5.4. Futile links are excluded from these CDFs because futile links cannot be improved by schemes. As expected, PPK performs dramatically better than PAN in this scenario. The fractions of non-futile links that exhibit SINR < 6 dB are listed in Table 5.4. Compared with PAN, PPK decreases the fractions of non-futile links that exhibit SINR < 6 dB. This is due to the use of reflected-ray paths and the removal of interference from futile links. The improvement does not vary significantly with M.

CDFs of DN-position power are presented in Figure 5.5. DN-position powers are lower with PPK than with PAN. This is due to the removal of interference from futile links. This effect decreases with increasing M. This is due to the higher amount of interference produced in networks with higher M.

5.3 GPK in Residential Terrain

In the previous section, we demonstrated the improvement gained by accounting for terrain. Now we consider global optimization accounting for terrain. The global scheme presented in this section is referred to as the "Global assuming Perfect Knowledge of terrain" (GPK) scheme. GPK determines tentative pointings using PPK, and then performs an optimization that is identical to that of GAN (Chapter 3). Specifically:

- Receiver beams point along the tentative pointings determined by PPK, and no attempt is made to optimize these.

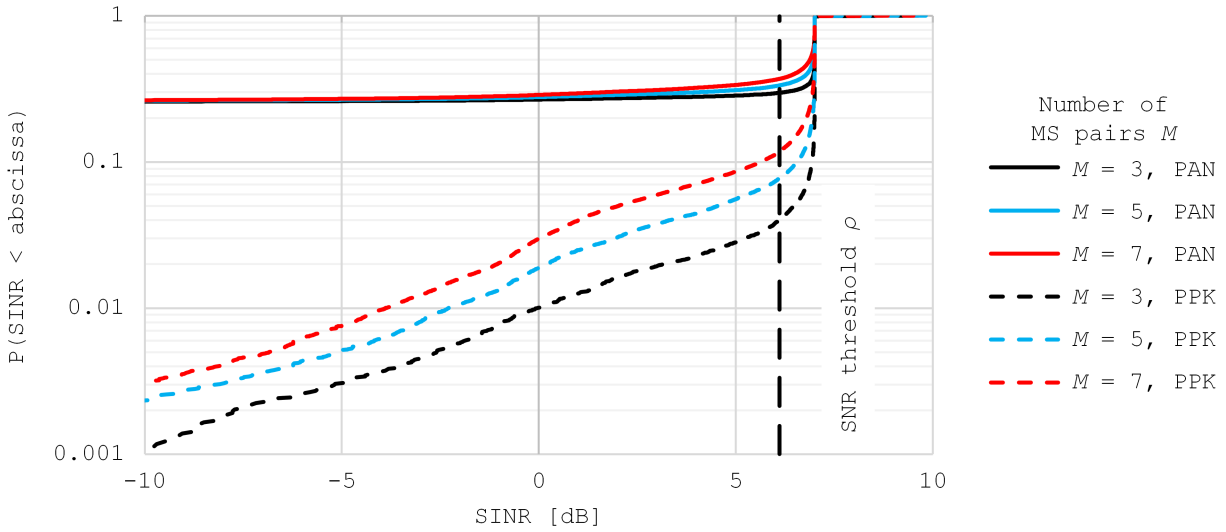

Figure 5.4: CDFs of non-futile link SINR for PAN and PPK in residential terrain.

Number of MS pairs M	**Non-futile links that exhibit SINR < 6 dB**		
	PAN	PPK	Difference
3	29.5%	3.8%	−25.7%
5	33.0%	7.4%	−25.6%
7	36.5%	11.2%	−25.3%

Table 5.4: Fractions of non-futile links that exhibit SINR < 6 dB for PAN and PPK in residential terrain.

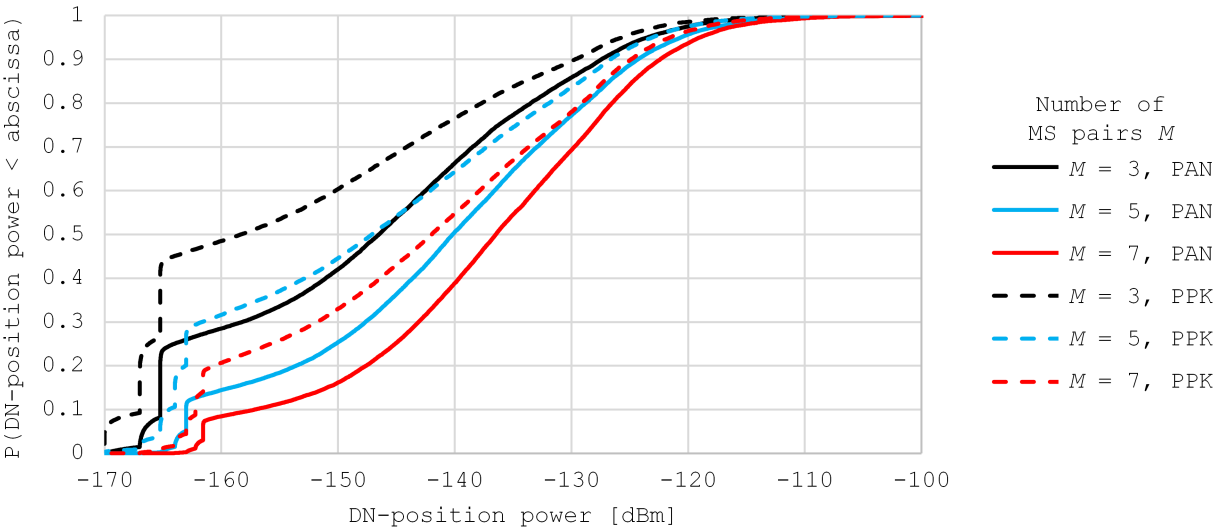

Figure 5.5: CDFs of DN-position power for PAN and PPK in residential terrain.

- As in GAN, transmitter beams may point either along the tentative pointing determined with PPK, or along one from nine pointings over about a beamwidth around the tentative pointing determined with PPK, i.e., $\Delta_\phi = 2.5°$ as described in Section 3.4. GPK will use set 5 of candidate solution sets listed in Table 3.2.

- As in GAN, A is calculated to make the associated receiver MS's SNR equal to ρ, i.e., interference is not considered in this calculation. When multiple paths exist between an MS pair, the received power from all the paths could be considered when setting A. For simplicity, we only consider the power from the path associated with the tentative pointing determined with PPK. Considering all paths would make the calculation of the power factor β (compensating for the loss due to off-pointing) ambiguous. Specifically, the change in antenna gain due to pointing away from the pointing determined with PPK would be different for each path, and therefore the required value of β would vary between paths. Finally, A for non-futile links is set as follows (repeating Equation 3.9):

$$A \leftarrow \frac{\rho N \alpha \beta L}{G_T G_R} \tag{5.2}$$

  For futile links, $A \leftarrow 0$.

As shown in Section 3.6, restricting the number of candidate solutions as described above might result in none of the candidate solutions meeting all constraints, or multiple candidate solutions yielding the same $\min(\max(\mathbf{A}))$. GPK selects a solution using the same process as the one used by GAN, which is described in Section 3.2 (Equation 3.3).

To demonstrate the performance of GPK, we repeat the experiment in Section 5.1 with GPK. CDFs of non-futile link SINR are presented in Figure 5.6. The fractions of non-futile links that exhibit SINR < 6 dB are listed in Table 5.5. Compared with PPK, GPK decreases the fractions of links that exhibit SINR < 6 dB. This is due to a decrease in interference from adjusting transmitter MS pointings and powers. This effect is greater in networks with higher M. This is due to the higher amount of interference produced in networks with higher M.

The fractions of realizations where GPK "falls back" to the unconstrained optimiza-

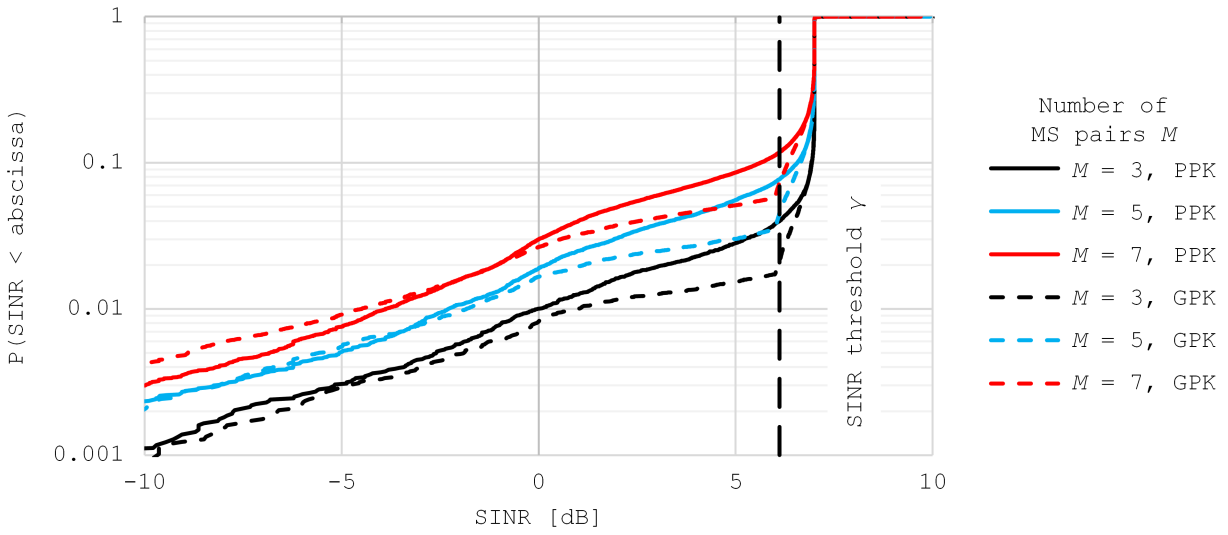

Figure 5.6: CDFs of non-futile link SINR for PPK and GPK in residential terrain.

Number of MS pairs M	**Non-futile links that exhibit SINR < 6 dB**		
	PPK	GPK	Difference
3	3.8%	1.7%	−2.1%
5	7.4%	3.5%	−3.9%
7	11.2%	5.7%	−5.5%

Table 5.5: Fractions of non-futile links that exhibit SINR < 6 dB for PPK and GPK in residential terrain.

tion problem (Equation 3.3) are listed in Table 5.6. The fractions for GAN in null terrain are included for comparison. As in GAN, the high fractions suggest the quantization of candidate solutions limits the extent to which the solution can be optimized. As in GAN, these fractions of realizations increase with increasing M. Again, this is due to the quantization of candidate solutions. Excluding the pointing determined with PPK, each transmitter MS candidate pointing has a complementary candidate pointing with the same β, i.e., transmitter MS antennas can point either clockwise or counter-clockwise about the pointing determined with PPK by one of the specified offsets. Thus, GPK falls back to Equation 3.3 to select between complementary candidate solutions when one of the transmitter beams point away from the pointing determined with PPK. Since networks with higher M are more likely to have a transmitter MS beam point away from the pointing determine with PPK, the fractions of realization where GPK falls back on Equation 3.3 increases with increasing M.

Number of MS pairs M	**Realizations where scheme falls back to Equation 3.3**		
	GAN in null terrain	GPK in residential terrain	Difference
3	97.8%	94.6%	−2.9%
5	99.9%	99.4%	−0.5%
7	100.0%	99.9%	−0.1%

Table 5.6: Fractions of realizations where scheme falls back to Equation 3.3 for GAN in null terrain and GPK in residential terrain.

CDFs of DN-position power are presented in Figure 5.7. Compared with PPK, GPK does not significantly affect performance in this aspect. As with PPK, DN-position powers increases as M increases. This is due to the higher amount of interference produced in networks with higher M.

The realization runtimes for GPK are listed in Table 5.7. The realization runtimes for PPK are included for comparison. As expected, the difference between PPK and GPK increases with increasing M. This is due to exponentially increasing number of calculations required for GPK in networks with increasing M.

5.4 Conclusions

PPK (Section 5.2) and GPK (Section 5.3) are schemes that use knowledge of the terrain to select MS pointings and powers. Networks with these schemes were simulated in residential terrain (as described in Section 5.1 and and the Appendix). The performance of PPK and GPK on link SINR is presented in Figure 5.6. Compared with PPK, GPK significantly decreased the fractions of links that exhibit SINR < 6 dB (Table 5.5). The performance of PPK and GPK on DN-position power is presented in Figure 5.7. Compared with PAN, PPK significantly increased DN-position power (Figure 5.5). Compared with PPK, GPK does not significantly affect performance in this aspect (Figure 5.7).

The performance improvements of GPK relative to PPK are similar to those of GAN relative to PAN. The fractions of links that exhibit SINR < 6 dB for PPK and GPK in residential terrain (from Table 5.5) and PAN and GAN in null terrain (from Tables 2.3 and 3.5) are

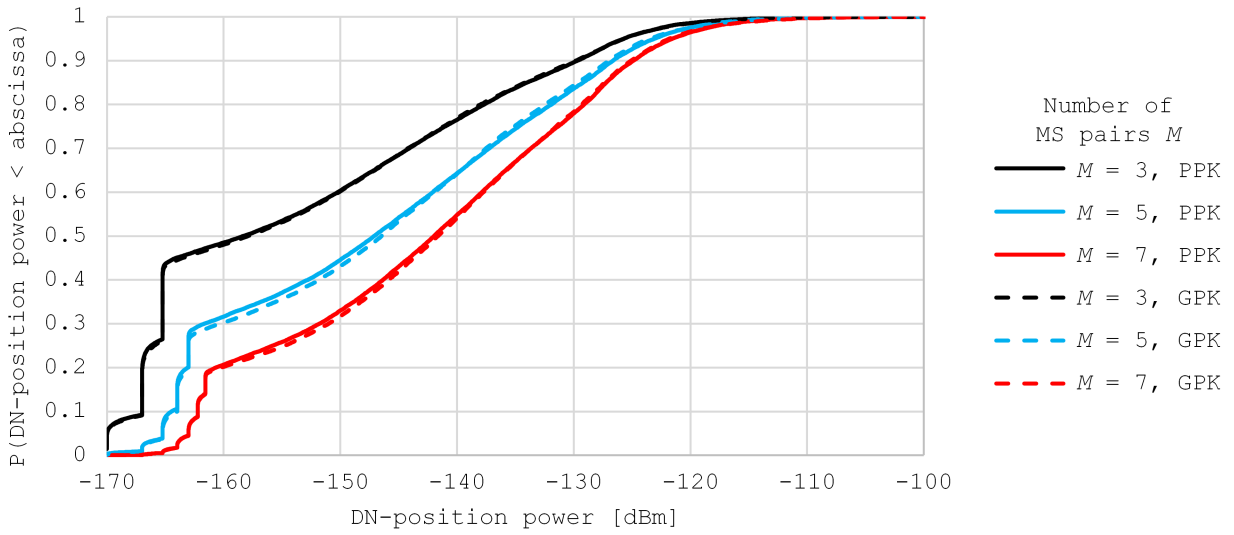

Figure 5.7: CDFs of DN-position power for PPK and GPK in residential terrain.

Number of MS pairs M	**Realization runtimes from simulations**		
	PPK	GPK	Difference
3	$\sim$ 4 ms	$\sim$ 26 ms	22 ms
5	$\sim$ 8 ms	$\sim$ 67 ms	59 ms
7	$\sim$ 11 ms	$\sim$ 2,992 ms	2,981 ms

Table 5.7: Realization runtimes t_R for PPK and GPK in residential terrain.

repeated in Table 5.8. Compared with their corresponding pairwise schemes, GAN and GPK significantly improve the fractions of links that exhibit SINR < 6 dB. The magnitudes of these improvements are similar. Compared with their respective pairwise schemes, GAN and GPK did not significantly affect the fractions of DN-position power.

The realization runtimes of PPK and GPK in residential terrain (from Table 5.7) and PAN and GAN in null terrain (from Table 3.7) are repeated in Table 5.9. The differences in realization runtime between the global schemes and their respective pairwise schemes is less than 3 seconds for networks with three, five, and seven MS pairs.

Number of MS pairs M	**Non-futile links that exhibit SINR $<$ 6 dB**					
	Null terrain			**Residential terrain**		
	PAN	GAN	Difference	PPK	GPK	Difference
3	2.8%	0.7%	−2.1%	3.8%	1.7%	−2.1%
5	5.8%	1.0%	−4.8%	7.4%	3.5%	−3.9%
7	8.4%	2.6%	−5.8%	11.2%	5.7%	−5.5%

Table 5.8: Fractions of non-futile links that exhibit SINR $<$ 6 dB for varying schemes in varying terrains.

Number of MS pairs M	**Realization runtime**					
	Null Terrain			**Residential Terrain**		
	PAN	GAN	Difference	PPK	GPK	Difference
3	$<$ 1 ms	$<$ 1 ms	0 ms	4 ms	26 ms	22 ms
5	$<$ 1 ms	36 ms	35 ms	8 ms	67 ms	59 ms
7	$<$ 1 ms	2,422 ms	2,422 ms	11 ms	2,992 ms	2,981 ms

Table 5.9: Realization runtimes for varying schemes in varying terrains.

Chapter 6

Conclusions

In this thesis, we explored coordinated beamforming in terrestrial mobile peer-to-peer millimeter wave networks. Networks with varying numbers of links were simulated in terrains with and without obstructions. Our coordinated beamforming schemes significantly improved SINR statistics. These results are summarized in Table 5.8. Greater improvement was found in networks with higher numbers of links and in networks in terrain with obstructions.

In this chapter, we elaborate on the contributions of this thesis, discuss considerations that might be relevant for future work, and suggest future work. This chapter is organized as follows. Contributions of this thesis are summarized in Section 6.1. Additional considerations that might be relevant for future work are presented in Section 6.2. Suggestions for future work are presented in Section 6.3.

6.1 Contributions

The contributions of this thesis are summarized as follows:

- Developed computationally tractable schemes for coordinated beamforming in terrestrial mobile peer-to-peer millimeter wave networks, specifically GAN (Sections 3.2-3.5) and

GPK (Section 5.3). The computational burdens of these schemes were quantified and are summarized in Table 5.9.

- Showed the efficacy of coordinated beamforming in null terrain (Figure 3.9 and Table 3.5) and residential terrain (Figure 5.6 and Table 5.5). The residential terrain is defined in the Appendix.

- Developed procedures and associated software to generate results presented in this thesis. The simulation process is described in Section 2.1. The terrain and propagation models are presented in Sections 2.1 and 4.1.

6.2 Additional Considerations

Additional considerations that might be relevant for future work are listed as follows.

MS Position Uncertainty. In our simulations, we assume perfect mobile station (MS) position information is available. However, position uncertainty is inevitable. In particular, the position precisions of global navigation satellite systems are typically on the order of a few meters to tens of meters. The performance of our schemes will degrade due to position uncertainty.

Terrain Uncertainty. In our simulations, we assume that perfect terrain knowledge is available. However, terrain uncertainty is inevitable. The performance of our schemes will degrade due to terrain uncertainty.

Latency. Our schemes require information to be acquired by MSs and uploaded to the network, and beam pointings and transmitter powers must be selected and downloaded to MSs. This cycle must be completed in less time than it takes for the network to significantly change; in particular, in less time than it takes for MS positions and terrain to significantly change. For example, this cycle must be completed within 30 ms for ~ 1 m MS position accuracy for MSs traveling at 100 km/hr. The performance of our schemes will degrade if their latency is greater than this. Some initial work in this direction is presented in [14].

Beam Scanning. Beam scanning is beam alignment by testing many pointings over a broad angular range. As mentioned in Chapter 1, millimeter wave networks will likely employ some form of beam scanning. Ideally, our schemes could replace beam scanning, as described earlier. However, beam scanning will be required when the performance of our schemes degrade due to position uncertainty or terrain uncertainty, or when the latency of our schemes is greater than that of beam scanning. Thus, rather than replacing beam scanning, our schemes could enhance it. For example, when the solution space for a scan is large, our schemes could be used to limit the number of pointings to be tested.

6.3 Future Work

Suggested directions for future work are as follows.

Alternative Optimization Problem. Investigate alternative formulations of the constrained optimization problem for coordinated beamforming schemes. Alternative formulations such as those presented in Section 3.1 facilitate methods of solution that would dramatically reduce computational effort.

Smarter Searching. Investigate alternative search methods to the "brute-force" search methods considered in this study. Brute-force search is computationally intensive. As a result, we needed to arbitrarily and significantly constrain the solution space of our searches. Other search methods, e.g., particle swarm optimization (see e.g. [15]), might be less computationally intensive, thus enabling searches over larger solution spaces with less computational burden.

Progressive Searching. Investigate transferring results from previous solutions to future solutions. Previous solutions could be used to anticipate a smaller range of future solutions, requiring less computational effort.

Terrain Discovery. Investigate using feedback from data gathered from mobiles to detect terrain, as opposed to assuming perfect *a priori* knowledge. For example, if GAN were used in residential terrain, some assumed LOS paths would be blocked. This could be detected as a

lower than expected signal being received at a receiver MS. Also, beamforming arrays can be used to determine angle of arrival of waves. This would reveal also reflected paths, which could be analyzed to determine the shapes and locations of obstructions. Results from this type of analysis could be used to make terrain maps, so that complete *a priori* terrain knowledge is not required. Some initial work in this direction is reported in [16].

Dynamic Terrain Discovery. Investigate using feedback from previous solutions to discover *changes* in terrain. For example, a vehicle might move into or out of a location that blocks a LOS path. This would be manifested as an unexpected change in signal being received at a receiver MS. This information could be used to update terrain maps.

A Appendix: Definitions of Terrains with Obstructions

The terrain used to demonstrate the propagation model defined in Chapter 4 is shown in Figure A.1. Residential terrain simulated in Chapter 5 is shown in Figure A.2. Obstructions are modeled as rectangles. The vertexes of the rectangles are listed in Tables A.1 and A.2. For each vertex, there is a vector pointing to an adjacent vertex, thereby defining the perimeter of the obstruction. The set of positions to which mobile station (MS) positions are restricted in the residential terrain is defined in Table A.3 in the same manner, i.e., as a set of vertices with associated vectors pointing to an adjacent vector.

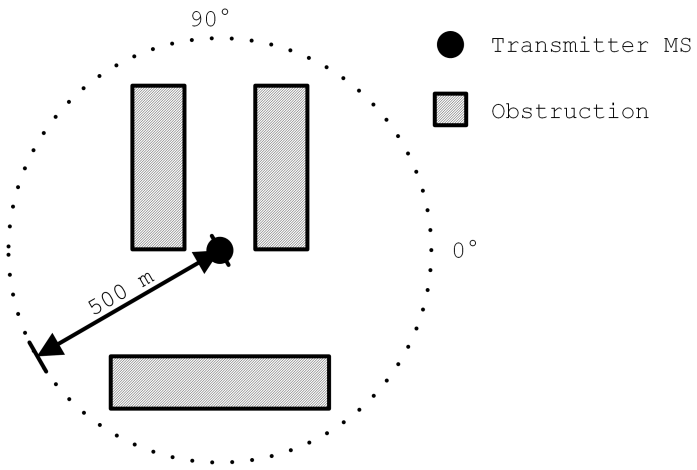

Figure A.1: Terrain used to demonstrate propagation model with obstructions.

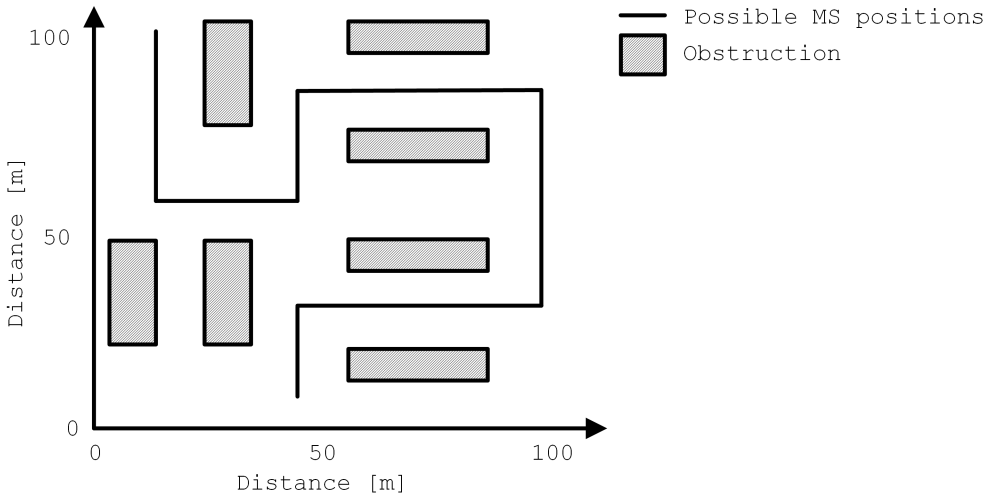

Figure A.2: Residential terrain.

Anchor Point (x, y) **[m]**	**Vector** $(\hat{x}, \hat{y})$
$(50, -0.1)$	$(0, 400)$
$(50, 399.9)$	$(100, 0)$
$(150, 399.9)$	$(0, -400)$
$(150, -0.1)$	$(-100, 0)$
$(-150, -0.1)$	$(0, 400)$
$(-150, 399.9)$	$(100, 0)$
$(-50, 399.9)$	$(0, -400)$
$(-50, -0.1)$	$(-100, 0)$
$(-200, -400)$	$(0, 100)$
$(-200, -300)$	$(400, 0)$
$(200, -300)$	$(0, -100)$
$(200, -400)$	$(-400, 0)$

Table A.1: Obstruction information for terrain used to demonstrate propagation model defined in Chapter 4.

Anchor Point (x, y) **[m]**	**Vector** $(\hat{x}, \hat{y})$
$(0, 20)$	$(0, 30)$
$(0, 50)$	$(10, 0)$
$(10, 50)$	$(0, -30)$
$(10, 20)$	$(-10, 0)$
$(20, 20)$	$(0, 30)$
$(20, 50)$	$(10, 0)$
$(30, 50)$	$(0, -30)$
$(30, 20)$	$(-10, 0)$
$(20, 80)$	$(0, 30)$
$(20, 110)$	$(10, 0)$
$(30, 110)$	$(0, -30)$
$(30, 80)$	$(-10, 0)$
$(50, 10)$	$(0, 10)$
$(50, 20)$	$(30, 0)$
$(80, 20)$	$(0, -10)$
$(80, 10)$	$(-30, 0)$
$(50, 40)$	$(0, 10)$
$(50, 50)$	$(30, 0)$
$(80, 50)$	$(0, -10)$
$(80, 40)$	$(-30, 0)$
$(50, 70)$	$(0, 10)$
$(50, 80)$	$(30, 0)$
$(80, 80)$	$(0, -10)$
$(80, 70)$	$(-30, 0)$
$(50, 100)$	$(0, 10)$
$(50, 110)$	$(30, 0)$
$(80, 110)$	$(0, -10)$
$(80, 100)$	$(-30, 0)$

Table A.2: Obstruction information for residential terrain.

Anchor Point (x, y) **[m]**	**Vector** $(\hat{x}, \hat{y})$
$(10, 110)$	$(0, -50)$
$(10, 60)$	$(30, 0)$
$(40, 60)$	$(0, 30)$
$(40, 90)$	$(50, 0)$
$(90, 90)$	$(0, -60)$
$(90, 30)$	$(-50, 0)$
$(40, 30)$	$(0, -30)$

Table A.3: Track defining possible MS positions for residential terrain.

Bibliography

[1] T. S. Rappaport, S. Sun, R. Mayzus, H. Zhao, Y. Azar, K. Wang, G. N. Wong, J. K. Schulz, M. Samimi, and F. Gutierrez, "Millimeter Wave Mobile Communications for 5G Cellular: It Will Work!," *IEEE Access*, vol. 1, pp. 335–349, 2013.

[2] J. Choi, V. Va, N. Gonzalez-Prelcic, R. Daniels, C. R. Bhat, and R. W. Heath, "Millimeter-Wave Vehicular Communication to Support Massive Automotive Sensing," *IEEE Communications Magazine*, vol. 54, no. 12, pp. 160–167, 2016.

[3] Q. Ye, M. Al-Shalash, C. Caramanis, and J. G. Andrews, "Resource Optimization in Device-to-Device Cellular Systems Using Time-Frequency Hopping," *IEEE Transactions on Wireless Communications*, vol. 13, no. 10, pp. 5467–5480, 2014.

[4] W. Stutzman and G. Thiele, *Antenna Theory and Design*. Hoboken, NJ: John Wiley and Sons, 3rd ed., 2013.

[5] S. Saunders and A. Aragón-Zavala, *Antennas and Propagation for Wireless Communication Systems*. Hoboken, NJ: John Wiley and Sons, 4th ed., 2007.

[6] B. Lathi and Z. Ding, *Modern Digital and Analog Communicaion Systems*. New York, NY: Oxford University Press, Inc, 4 ed., 2009.

[7] Zukang Shen, J. G. Andrews, and B. L. Evans, "Optimal power allocation in multiuser OFDM systems," in *GLOBECOM '03. IEEE Global Telecommunications Conference*, vol. 1, pp. 337–341, 2003.

[8] R. Zakhour and S. V. Hanly, "Min-Max Power Allocation in Cellular Networks With Coordinated Beamforming," *IEEE Journal on Selected Areas in Communications*, vol. 31, no. 2, pp. 287–302, 2013.

[9] T. S. Rappaport, Y. Xing, G. R. MacCartney, A. F. Molisch, E. Mellios, and J. Zhang, "Overview of Millimeter Wave Communications for Fifth-Generation (5G) Wireless Networks—With a Focus on Propagation Models," *IEEE Transactions on Antennas and Propagation*, vol. 65, no. 12, pp. 6213–6230, 2017.

[10] T. S. Rappaport, G. R. MacCartney, S. Sun, H. Yan, and S. Deng, "Small-Scale, Local Area, and Transitional Millimeter Wave Propagation for 5G Communications," *IEEE Transactions on Antennas and Propagation*, vol. 65, no. 12, pp. 6474–6490, 2017.

[11] M. Jacob, S. Priebe, R. Dickhoff, T. Kleine-Ostmann, T. Schrader, and T. Kurner, "Diffraction in mm and Sub-mm Wave Indoor Propagation Channels," *IEEE Transactions on Microwave Theory and Techniques*, vol. 60, no. 3, pp. 833–844, 2012.

[12] S. S. Zhekov, O. Franek, and G. F. Pedersen, "Dielectric Properties of Common Building Materials for Ultrawideband Propagation Studies [Measurements Corner]," *IEEE Antennas and Propagation Magazine*, vol. 62, no. 1, pp. 72–81, 2020.

[13] Z. Yun and M. F. Iskander, "Ray Tracing for Radio Propagation Modeling: Principles and Applications," *IEEE Access*, vol. 3, pp. 1089–1100, 2015.

[14] S. W. Ellingson, "Continuous updating of radio environment maps for millimeter-wave networks with beamforming," in *2017 IEEE International Symposium on Antennas and Propagation*, pp. 937–938, July 2017.

[15] L. Zhu, J. Zhang, Z. Xiao, X. Cao, D. O. Wu, and X. Xia, "Joint Tx-Rx Beamforming and Power Allocation for 5G Millimeter-Wave Non-Orthogonal Multiple Access Networks," *IEEE Transactions on Communications*, vol. 67, no. 7, pp. 5114–5125, 2019.

[16] S. W. Ellingson and A. Marinkovich, "Discovery of Blocking Terrain in a Millimeter- Wave Network by On-the-Fly Incoherent Tomography," in *2018 IEEE International Symposium on Antennas and Propagation*, pp. 1923–1924, July 2018.